

Introduction of a Biologically Plausible Color Descriptor to a Neurodynamical Model of the Primary Visual Cortex

Sean Thomas Connolly

Abstract

We present a computational model of color description & processing in the primary visual cortex (V1), inspired by current neurobiological understanding. This understanding posits single and double-opponent neurons as fundamental to low level color processing. We offer a novel representation of color by defining these cells' responses and the connections between them, within the framework of a dynamical model of neuronal activity. Our model reproduces perceptual experiences in a number of cases, offering credence to said biological theories.

Index Terms

primary visual cortex, striate cortex, V1, receptive field, single-opponent, double-opponent, color induction

I. INTRODUCTION

PERCEPTION of color is defined not just by the physical properties of the object, but also the context in which it is viewed. Taking advantage of this, we can create a wealth of optical illusions in which two physically identical stimuli are made to appear as different colors, or two physically different stimuli are made to appear the same, simply by changing the spatial or temporal context [3]. Consider Figure 1, for example. Here we see that two physically identical turquoise rings can be perceived as very different, depending solely on the context in which they are viewed. Two interesting questions arise: why has our color vision evolved to see things ‘not as they are’, and what are the underlying mechanisms at play?

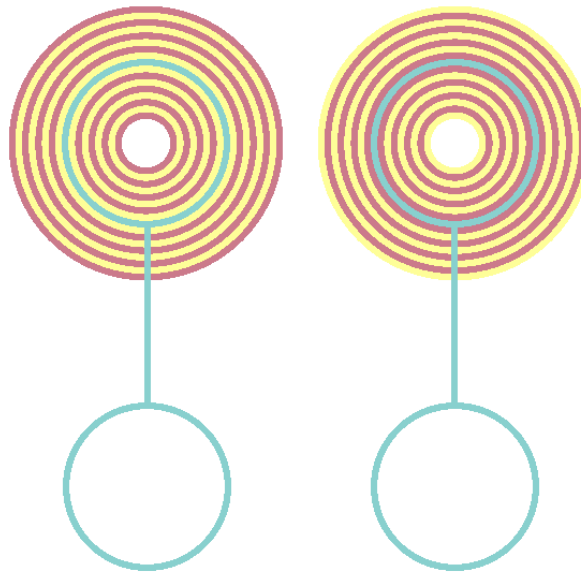


Figure 1: Example of contextual influences on the perception of color. The colors of the all rings on the left are physically identical to those on the right. The order of the rings differs, however. On the left, the test ring borders two yellow rings, while on the right the test ring borders two red rings. This change in context is what defines the perceived difference.

Neurophysiological research in the past decade or so has witnessed a growing confidence in the community that these phenomena begin to arise as early in primate vision processing as the primary visual cortex (V1) [3], [6], [16], [19], [18], [21]. It is believed that the processing of color and form in V1 are the beginnings of, amongst other effects, color constancy: the ability to perceive an object's color despite ambient luminance changes. This phenomenon has clear evolutionary benefits, such as the ability to recognize the color of ripe fruit even though the color of daylight might be changing from blue to red as the sun sets. Truly, as the ambient light changes, so too does the spectral reflectance of the fruit. Still, its color appears perceptually consistent. It has also been suggested that the processing of color and context in V1 may assist in defining object saliency [10]: the pre-attentive 'importance' of an object.

With respect to the underlying mechanisms, many have proposed that it is the *boundaries* between colored regions which drive the processing of color in V1 [3], [6], [16], [19], [18], [21] and, as a consequence, these phenomena. This can be observed in Figure 1 where it is the border between the turquoise rings and their neighboring rings that determines if they, the turquoise rings, are perceived as green or blue. Specifically, to explain this influence of form on color processing in V1, the literature proposes two broad classifications of neurons: single-opponent cells & double-opponent cells [6].

Opponency, in neurobiology, refers to antagonistic inputs of information: one source of input excites the neuron, while another inhibits it. These two antagonistic components are commonly referred to as the *on* and *off* inputs to a neuron. One can think of these two inputs as being what the cell 'is looking for', *on*, and what the cell 'is not looking for', *off*. Intuitively, stimulation from the *on* input excites the neuron, while stimulation from the *off* input inhibits it. Perhaps less intuitively, removal of stimulation from the *off* input also excites the neuron. This behavior is logical when you consider that the two antagonistic inputs typically represent mutually exclusive features. In this way, removal of the negative stimulus often means much the same as presence of a positive stimulus and thus it contributes to excitation of the neuron. Of course, if equal stimuli are provided from both the *on* and *off* inputs, excitation is cancelled out by inhibition and the neuron does not fire. Lastly, recognize that any one neuron usually receives antagonistic input from, in fact, many other neurons. The aggregate stimuli from these excitatory and inhibitory inputs determines if the cell fires.

With respect to cells in the early visual system, we specifically use opponency to refer to chromatic and spatial components. In Section II-A we detail what exactly this means, with specific examples of neurons' expected patterns of response to various stimuli, as well as the implications of such responses. To frame this explanation, consider for now that single-opponent cells respond best to *large areas* of color, while double-opponent cells respond only to the *boundaries* between such areas.

With this understanding of color and context in V1, we propose a computational model designed to describe color and the neurodynamical processes behind it. We present two implementations, one more biologically accurate and another more computationally elegant. We explore the behavior of these models with respect to what they can teach us about the assumed biological theories, as well as their application to the field of computer vision.

II. STATE OF THE ART

In order to frame our work, we wish to examine both the current understanding of the neurobiological mechanisms at play, as well as previous work in modeling these mechanisms. We present these reviews in the following sections, *A. Neurobiology* and *B. Computational Modeling*, respectively.

A. Neurobiology

Single-Opponent Neurons

Single-opponent cells are a class of neurons in the early visual system which respond best to large areas of color and/or luminance. Their behavior is achieved by constructing classical center-surround receptive fields. The center receptive field serves as the *on* input, exciting the cell when presented with a particular color, while the surround receptive field serves as the *off* input, inhibiting the cell when another color is present or exciting it when that color is removed. These center and surround receptive fields may involve very few retinal cones, or may span many degrees of vision [7].

In so called color preferring single-opponent cells, the cone inputs to the center and surround come from cones with different spectral response functions, e.g., L vs M. By arranging input from different cones into antagonistic receptive fields, we get a neuron which is sensitive to a particular color, in opposition to another. In the human visual system, we recognize three axes of such color opponency: redness vs. greenness, blueness vs. yellowness, and lightness vs. darkness. To construct these concepts of color, neurons in the visual pathway contrast activity of the three types of cone cells: those sensitive to long (L) wavelength light, those sensitive to medium (M) wavelength light, and those sensitive to short (S) wavelength light. By contrasting relative activity with neighboring L, M, and S cones, the retina itself can already begin to construct information resembling psychological concepts of 'color'.

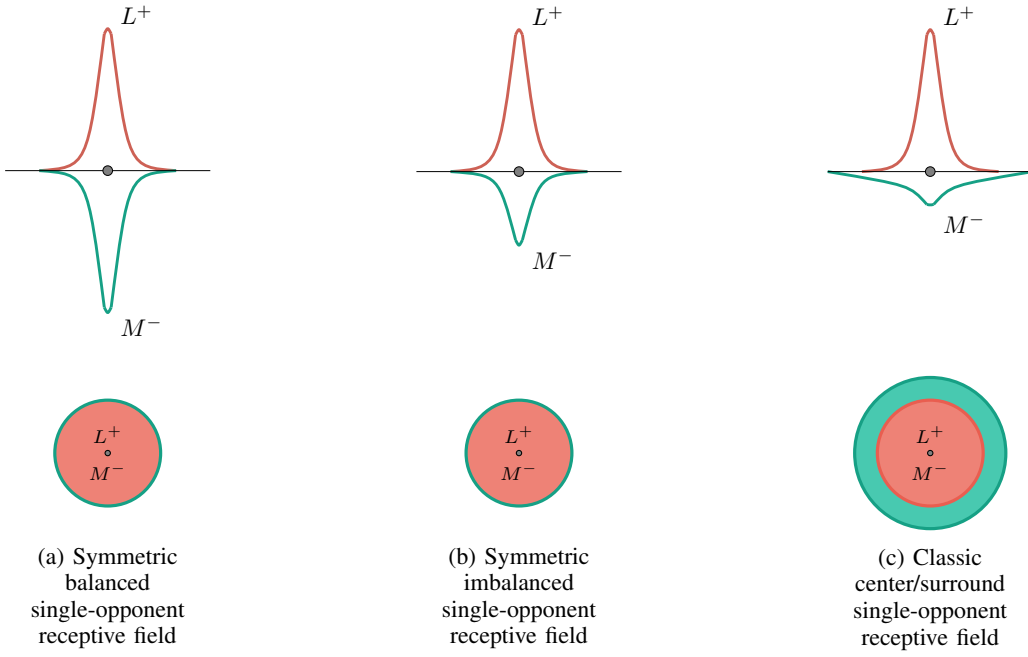


Figure 2: Examples of possible single-opponent receptive field configurations, many others could be designed. All function to describe color properties of surfaces, though their response patterns to similar stimuli vary slightly.

As mentioned, one of the three axes of the opponent process theory is lightness vs. darkness. This is achieved in single-opponent cells by providing opponent inputs into the *on* center and the *off* surround from the same cones. By including input of L, M, and/or S cones into both the center and surround, the cells becomes ‘color blind’ and instead only respond to changes in luminance [15]. Sometimes incorrectly labeled as ‘non-opponent’, these neurons are indeed single-opponent cells, specifically: achromatic single-opponent cells.

Double-Opponent Neurons

We have defined single-opponent cells to best respond to large areas of light/color. We now define double-opponent cells to respond only to the boundaries between such areas. In this regard, it is fair to think of double-opponent cells as biological ‘edge detectors’. However, there is disagreement about their precise definition in the literature. All parties involved in the discussion agree that the input to a double-opponent neuron is that of two single-opponent neurons itself. In this sense, the term “double-opponent” can be thought of as indicating that the dimensionality of color opponency has been increased. However, another camp of researchers take the definition a step further and suggest that the two single-opponent inputs are spatially offset. By this definition, the term “double-opponent” can imply that the cell is sensitive to opponency in two *different* dimensions: color and space. Schematics of the receptive fields of these two interpretations are presented in Figure 4.

The distinction is non-trivial as the response patterns differ significantly, and thus the interpretation of their role in vision differs. Truly, both types of cells may exist in the primate visual system. However, for the purpose of our work we only consider the latter definition: double-opponent cells’ receptive fields are both chromatically and spatially antagonistic, depicted in Figure 5.

Orientation Selectivity: Research shows that cells identified as double-opponent tend to be orientation selective [6], [19], [16], [15]. That is, they respond most strongly when stimulated by a border of particular orientation, less so with variation from that preferred orientation, and weakly, if at all, to borders orthogonal to the preferred orientation. This is intuitive given the organization of the receptive field as previously defined. By arranging the components of the receptive field to be spatially antagonistic, there will be one orientation of edge which best separates the two components, and another orientation, precisely orthogonal, which does not separate the two components at all. This can be easily visualized, as in Figure 6 and Figure 7.

It’s worth noting that a single-opponent neuron can also be selective to specific orientations. These cells have been identified in biology, though their relative abundance appears minimal [6]. To achieve orientation selectivity, the center and/or surround receptive fields simply need be non-circular. However, without the balanced asymmetric *on* and *off* receptive fields from each opponent cone(s), an orientation specific concentric single-opponent cell could never be as selective as a double-opponent cell.

Spatial Frequency Selectivity: Another important feature of double-opponent cells is that they are inherently selective to borders of specific ‘size’, or ‘scale’. Technically, we refer to such preference of ‘scale’ as a cell’s spatial frequency selectivity. Each double-opponent neuron will be selective to a particular spatial frequency and excited less so by stimuli of spatial frequency deviating from this preference. Again, this is intuitively a product of the design of the neuron’s receptive field and easily visualized, as in Figure 3.

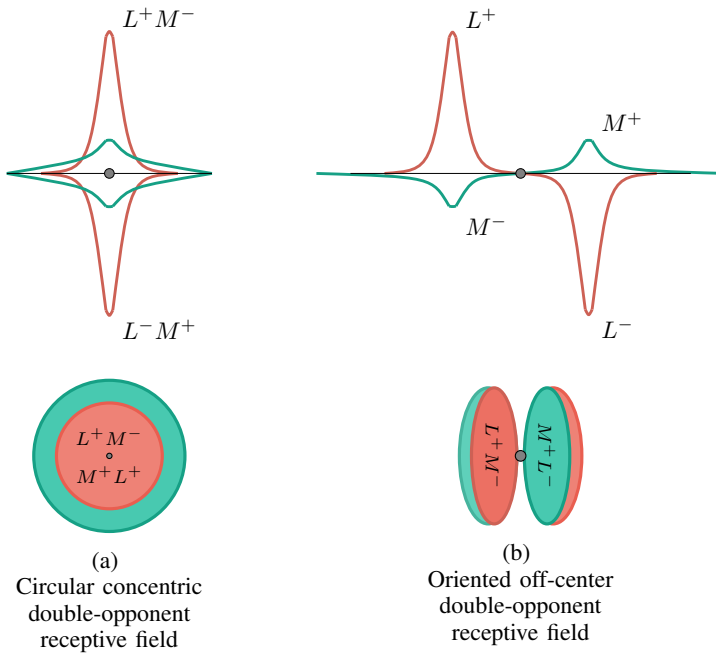


Figure 4: Comparison of the two different interpretations of double-opponent neuron receptive fields.

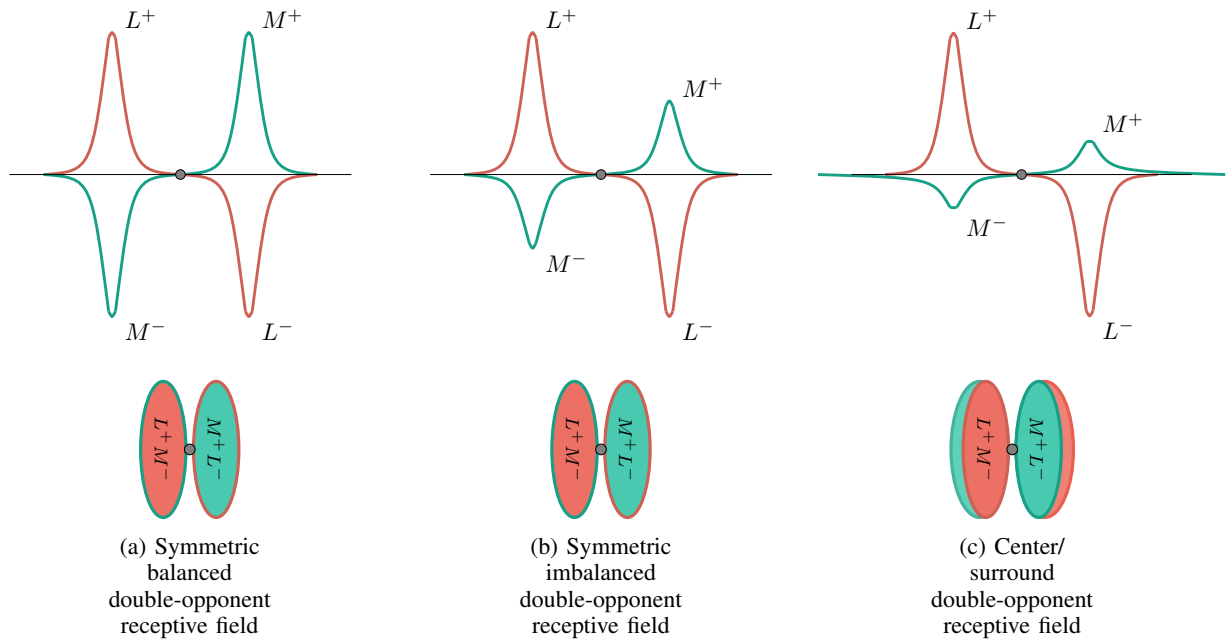


Figure 5: Examples of possible double-opponent receptive field configurations, many others could be designed. All function to describe color properties of borders, though their response patterns to similar stimuli vary slightly.

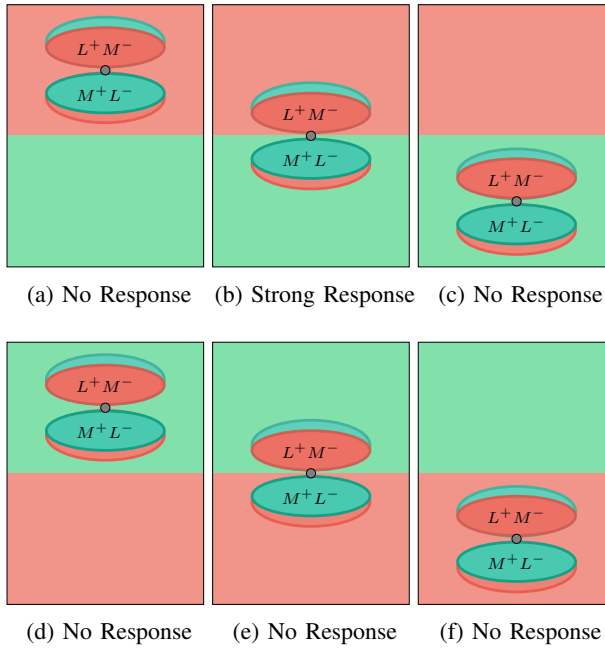


Figure 6: A double opponent cell selective to horizontally oriented borders with red above and green below; only responsive to that particular stimulus. In Figure (b), the neuron is presented with its ideal stimulus: its L^+ and M^+ receptive fields are fully activated while its L^- and M^- receptive fields are completely unactivated. Figure (e) presents the neuron with the exact opposite stimulus, neither its L^+ nor M^+ receptive fields are activate at all, and both its L^- and M^- receptive fields are fully activated, ensuring no response possible from the cell. While its L^+ receptive field might be strongly stimulated in (a) and (f), it's L^- receptive field cancels it out. Similarly, in (c) and (d) its M^+ receptive field is stimulated but cancelled out by activity in its M^- receptive field.

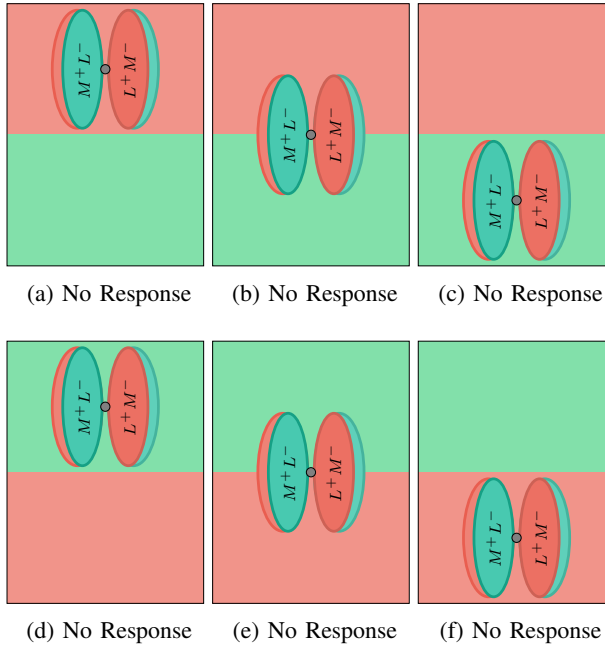


Figure 7: A double opponent cell selective to vertically oriented borders with red to the right and green on the left; completely unresponsive to a horizontal border. While its L^+ receptive field might be strongly stimulated in (a) and (f), it's L^- receptive field cancels it out. Similarly, in (c) and (d) its M^+ receptive field is stimulated but cancelled out by activity in its M^- receptive field. In (b) and (e) both of its L^+ and M^+ receptive fields are moderately activated, but again, cancelled out by activation in its L^- and M^- receptive fields, respectively.

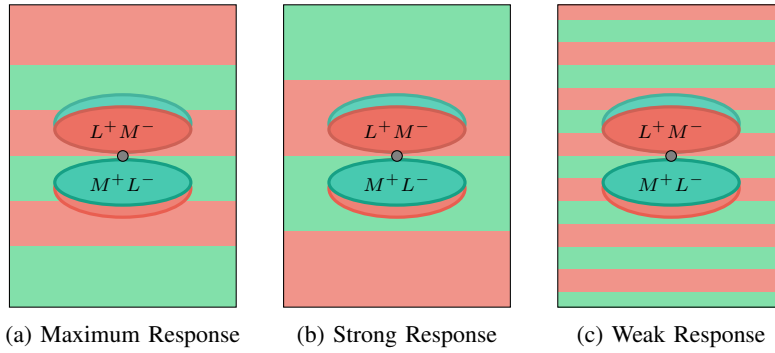


Figure 3: A double opponent cell tuned to a particular spatial frequency. Either (b) a lower or (c) a higher spatial frequency than preferred lowers the response of the cell.

As with single-opponent cells, one of the axes of the opponent process theory is ‘lightness’ vs ‘darkness’. While we frequently discuss opponency as being a thing of ‘color’, we find double-opponent cells which are specifically sensitive to luminance borders [6]. Such achromacy is easily achieved by balancing cone inputs into the neuron’s antagonistic receptive fields, as in single-opponent cells. It behaves just as the previously described double-opponent cells, with specific orientation and spatial frequency selectivity, but responds best to luminance borders rather than chromatic borders. For more details on achromatic receptive fields, please refer back to the section on achromatic single-opponent neurons. It is important to reiterate here that the *on* and *off* inputs to light and dark sensitive single-opponent cells are balanced, whereas their chromatic sensitive counterparts are imbalanced in inputs. This has the implication that light and dark double-opponent cells are, as defined, redundant. This can be seen in Figures 10a and 10b. This is in contrast to the chromatic double-opponent cells depicted in Figure 10 which differentiate themselves from their opponent pair by imbalanced inputs from the same cones.

Hypercolumns

Thus far we have defined two broad classes of neurons in the primate visual system: single-opponent and double-opponent. Each class has a number of parameters which dictate what stimuli the cell should respond to: opponent color, orientation selectivity, and spatial frequency. A single cell can only be sensitive to a specific combination of settings for each parameter. However, for each parameter it is important to have neurons sensitive to the full range of parameters. Thus, it is necessary to have a collection of neurons which together cover the complete combinatorial set of settings for all parameters.

Furthermore, as may be obvious, the receptive field of a neuron in V1 is directly responsive to a set of neurons in the retina. That is, neurons in V1 are sensitive only to activity at a particular physical location on the retina; V1 is *retinotopic*, or retinally mapped.

The implication is that for each retinal position, in V1 it is necessary to have a large number of both single-opponent and double-opponent cells, selective to the full gamut of parameters possible for each type of cell. Biologically, these collections of cells are organized in *hypercolumns*, a physical grouping of cells in which neuronal connections ‘up’ and ‘down’ within the column are much more dense than extensions to cells in other columns. Within a single hypercolumn, all cells are sensitive to a specific retinal location, but together express sensitivity to the full range of parameters.

B. Computational Modeling:

The model described in this research is an extension of that presented by Penacchio *et al.* [12], itself based on work by Li [9]. Before detailing our implementation, it is important to review prior art; these two works and others. As our goal is to model the behavior of achromatic and color preferring single-opponent and double-opponent neurons, we will also review other computational endeavors tackling the issue of color and/or form from a biologically inspired perspective.

Li’s Neurodynamical Model for Segmentation [9]

In Li’s original work, a neurodynamical model was presented which focused on global region segmentation using only local interactions between neurons. In the interest of simplicity, Li’s implementation dealt only with the nature of these interactions, ignoring where the stimulus, or information, might be coming from. Conceptually, Li defined neurons by their physical position in the image and the ‘feature’ to which they are sensitive. She then defined the connections between these neurons such that those physically close to each other, and sensitive to similar features, interacted most strongly. Stimulation of one neuron, then, positively stimulated (excited) similar neurons nearby, and negatively stimulated (inhibited) dissimilar neurons nearby. Such excitation and inhibition cascades through the network naturally, producing large scale response patterns defined only by local stimuli.

In the model presented, Li used oriented bars as features, though expressed that any logical feature could be reasonably considered in its place. This choice was biologically inspired by neurons sensitive to specifically oriented bars, the aforementioned double-opponent cells. When considering such features, inter-neuronal connections can be logically deduced: two neurons positively interact most when both 1) are sensitive to similarly oriented bars and 2) are co-located along that same orientation. Two neurons negatively interact most when either of these two conditions is not met.

By defining neuronal connectivity in this manner, patterns of neurons sensitive to co-located and co-aligned bars positively interact with each other to enhance their collective response to the stimuli. Similarly, incoherent stimuli negatively interact with their neighbors and are silenced. From these local interactions, global features are enhanced if they satisfy the connectivity rules, and noise is suppressed. Li showed that this method can be used to enhance contours and identify boundaries between regions for which normal segmentation methods struggle.

Penacchio, Otazu, & Dempere-Marcos Neurodynamical Model for Brightness Induction [12]

Li's work laid the foundation for Penacchio *et al.*, who extended and generalized the model to a flexible framework. Most importantly, they dealt with the question which Li had previously not: what is meaningful input to the neurodynamical model? In Li's model, neurons responded to oriented 'bars' which were, it is assumed, provided to the retinotopic neurodynamical model directly. Penacchio *et al.* utilized a discrete wavelet transform (DWT) [13] to decompose real images into their oriented multiresolution components, which then served as the input to Li's model.

In the context of the previously described neurobiology, this multiresolution decomposition, when applied to grayscale images, could be interpreted as modeling the response patterns of achromatic double-opponent cells. Their findings were positive as the neurodynamical model modeled the interactions between these cells, increasing saliency and simulating brightness induction (BI) phenomena at high contrast borders.

A byproduct of using a DWT to obtain input was that they did not just obtain oriented edge information, but multiresolution oriented edge information. This added another dimension to the hypercolumn model: for each retinotopic position, they modeled the activity and interactions of achromatic double-opponent cells with both orientation and spatial frequency selectivity. Introducing this extra dimension of input information required the specification of interactions between neurons of differing spatial frequency selectivity in the dynamical model.

As mentioned, our work is a direct continuation of this research line. Thus, we build on this model, introducing yet another dimension to the hypercolumn model: color. Similarly, it will be necessary that we introduce biologically meaningful interactions between neurons of differing chromatic selectivity to the dynamical model.

Itti, Koch, & Niebur's Model for Saliency [5]

Itti *et al.* implemented a biologically inspired model of visual attention, or saliency. This work included opponent processing of color, center/surround receptive fields at scales, and orientation selectivity. Because of these features, and their overlap with our own goals, we acknowledge it as an influential work.

In this model color is included by treating the RGB image as analogous for L, M, and S cone activity. From this Red, Green, Blue, and Yellow color components, as well as a single Intensity component is derived, using the following formulae:

$$\text{Intensity} = \frac{(L + M + S)}{3} \quad (1)$$

$$\text{Red} = \max(0, L - \frac{(M + S)}{2}) \quad (2)$$

$$\text{Green} = \max(0, M - \frac{(L + S)}{2}) \quad (3)$$

$$\text{Blue} = \max(0, S - \frac{(L + M)}{2}) \quad (4)$$

$$\text{Yellow} = \max(0, \frac{(L + M)}{2} - \frac{|(L + M)|}{2} - S) \quad (5)$$

Each of the L , M , and S (RGB) channels are normalized by I in order to decouple hue from intensity. These derived color components (and intensity) are computed for a set of images convolved in a *Gaussian pyramid* and contrasted across scales to obtain center/surround opponent color (and intensity) channels:

$$\text{Intensity}(c, s) = |I(c) \ominus I(s)| \quad (6)$$

$$\text{RedGreen}(c, s) = |(R(c) - I(s)) \ominus (G(s) - R(s))| \quad (7)$$

$$\text{BlueYellow}(c, s) = |(B(c) - Y(s)) \ominus (Y(s) - B(s))| \quad (8)$$

Itti *et al.* also compute orientation features by deconvolving I with oriented *Gabor pyramids* at scale $(O(\sigma, \theta))$. These responses are then contrasted across scales to obtain orientation feature maps $(O(c, s, \theta))$:

$$O(c, s, \theta) = |O(c, \theta) \ominus O(s, \theta)| \quad (9)$$

Biologically, such features could be considered representative of achromatic double-opponent cells. Similar to the features obtained by Penacchio *et al.*'s use of discrete wavelet transforms (DWT), they include information about the intensity, position, and orientation of edges.

This set of 42 feature maps; intensity at 6 scales, 2 opponent colors at 6 scales each, and 4 orientations at 6 scales each, provide input for a dynamical neural network. In their neurodynamical model of saliency, each point of the feature maps represents activity of a neuron and interactions between neurons ensure that only the most active locations remain, while all others are suppressed.

Yang, Gao, Li & Li's Model of Boundary Detection [23]

Yang *et al.* developed a biologically inspired system of edge detection. To this end, they implemented a model of chromatic double-opponent receptive fields constructed from asymmetric gaussian filters. The first step in their algorithm is to transform the RGB input image to red, green, blue, and yellow opponent color channels. Their approach simply utilizes the red, green, and blue color channels as they are, and define yellow to be the average of red and green input.

$$\text{Red} = R \quad (10)$$

$$\text{Green} = G \quad (11)$$

$$\text{Blue} = B \quad (12)$$

$$\text{Yellow} = \frac{R + G}{2} \quad (13)$$

These four color components are then convolved with centered, circular gaussian filters. This can be interpreted as modeling the receptive fields of chromatic single-opponent cells. These single-opponent cell responses are then combined in spatially opponent pairs to derive models of chromatic double-opponent cells.

For their purposes of boundary detection, they evaluate their modeling of double-opponent cells only, discarding single-opponent cell responses. However, their implementation of single-opponent cells is perfectly reasonable and taken as inspiration in our work. The primary shortcoming of the research by Zhang *et al.* lies in the description of color itself; while convenient, it is not supported by biology thus needs to be rethought.

Zhang, Barhomi, & Serre's Biologically Inspired Color Descriptor [24]

Zhang *et al.* introduce a computational color descriptor which integrates color and form. They specifically aim to model the behavior of single-opponent and double-opponent cells in the primate visual system. To do so, they consider the three classical opponent axes (Red-Green, Blue-Yellow, Light-Dark), as well as a fourth (Red-Cyan), omitted here.

Single-opponent cells' responses are modeled by first convolving the RGB input with a center (c) surround (s) filters, and then applying the following transformations:

$$\text{Light}(c, s) = \frac{1}{\sqrt{3}}L(c) + \frac{1}{\sqrt{3}}M(c) + \frac{-1}{\sqrt{3}}S(s) \quad (14)$$

$$\text{Dark}(c, s) = \frac{1}{\sqrt{3}}S(c) + \frac{-1}{\sqrt{3}}L(s) + \frac{-1}{\sqrt{3}}M(s) \quad (15)$$

$$\text{Red}(c, s) = \frac{1}{\sqrt{2}}L(c) + \frac{-1}{\sqrt{2}}M(s) \quad (16)$$

$$\text{Green}(c, s) = \frac{-1}{\sqrt{2}}L(s) + \frac{1}{\sqrt{2}}M(c) \quad (17)$$

$$\text{Blue}(c, s) = \frac{2}{\sqrt{6}}S(c) + \frac{-1}{\sqrt{6}}L(s) + \frac{-1}{\sqrt{6}}M(s) \quad (18)$$

$$\text{Yellow}(c, s) = \frac{1}{\sqrt{6}}L(c) + \frac{1}{\sqrt{6}}M(c) + \frac{-2}{\sqrt{6}}S(s) \quad (19)$$

In this work the team explored three means of modeling single-opponent centers and surrounds: gradient operator, Gabor filters, and Gaussian derivatives. It is important to note that each of these models of receptive fields were oriented, and thus the models of single-opponent neurons presented were, at least weakly, oriented.

To model double-opponent cell responses, the output from single-opponent cells are further convolved with a number of oriented filters. These convolutions are then summed over phase and opponent pairs to yield three spatially and chromatically opponent channels; Light-Dark, Red-Green, and Blue-Yellow (as well as Red-Cyan in their work).

The output of their model is a set of feature maps representing the response patterns of single-opponent and double-opponent neurons selective to specific orientations. Thus, this work is particularly influential to ours.

Spitzer & Barkan's Model of Color Induction [22]

Spitzer *et al.* implemented a computational model of color induction by processing center and surround receptive fields of single and double-opponent neurons. While we also aim to model color induction, as well as brightness induction, our approach differs significantly from theirs. Our model seeks to introduce induction effects primarily through its neurodynamical component, while theirs relies mostly on center and surround (and remote) effects introduced by the cells' receptive fields, as well as a temporal adaptation function.

Another important difference is that their implementation considered double-opponent cells to be circular concentric. That is, they accepted the definition of double-opponent cells which we discarded in our research (see *Double-Opponent Neurons* above). Using this definition of double-opponent cells, Spitzer *et al.* were able to model well chromatic induction and simultaneous contrast effects, though their model was not sensitive to oriented edges.

In their model they defined four opponent color components; red, green, blue, and yellow:

$$Red(c, s) = L(c) - M(s) \quad (20)$$

$$Green(c, s) = M(c) - L(s) \quad (21)$$

$$Blue(c, s) = S(c) - \frac{L(s) - M(s)}{2} \quad (22)$$

$$Yellow(c, s) = \frac{L(c) - M(c)}{2} - S(s) \quad (23)$$

This definition of the opponent color process seems, to us, more biologically plausible than those presented by Itti *et al.* [5], Yang *et al.* [23], or Zhang *et al.* [24]. Thusly, it will form the basis for our opponent color transformation, presented in the *Method* section below.

Comparison of Models

Our current work is a direct continuation of the research presented in the first two of these computational models. The latter four represent but a small selection of the wealth of effort being put into computationally describing color in a biologically plausible manner. It is important to recognize that these five models each had different specific research goals and so do not intend to be directly compared to one another. We present them here to frame our current work. Table ?? presents the features implemented in these models with respect to the goals of our work. This comparison elucidates our intentions: to bring biologically inspired descriptions of color to the neurodynamical processing model developed by Penacchio [12] and Li [9].

TABLE I: Comparison of computational models relevant to our current work.

	Proposed Model	Penacchio [12]	Li [9]	Itti [5]	Spitzer [22]	Yang [23]	Zhang [24]
Dynamical Intensity	Y Y	Y Y	Y N	Y Y	Y N	N N	N Y
Colors	Y	N	N	Y	Y	Y	Y
Scales	Y	Y	N	Y	N	Y	N
Orientations	Y	Y	Y	Y	N	Y	N
SO	Y	N	N	Y	Y	Y	Y
DO	Y	Y (achromatic)	N	Y	Y (concentric)	Y	Y
SO RF	Gaussian / DWT	N/A	N/A	Gaussian Pyramid	Gaussian	Gaussian	Difference of Gaussians
DO RF	Gabor-like Gaussians / DWT	DWT	N/A	Gabor Pyramid	Gabor	Gabor-like Gaussians	Difference of Gaussians
Goal	Color Induction	Brightness Induction	Saliency	Saliency	Color Induction	Edge Detection	Color Descriptor
Definition of criteria:	Dynamical: Does the work attempt to model neurodynamical processes? Intensity: Does the work consider achromatic differences as features? Colors: Does the work consider chromatic differences as features? Scales: Does the work separate information at different scales? Orientations: If incorporating edge/boundary features, does the work distinguish between orientations? SO: Does the work attempt to model single-opponent cell behavior, directly or indirectly? DO: Does the work attempt to model double-opponent cell behavior, directly or indirectly? SO RF: If modeling single-opponent cells, how are their receptive fields defined? DO RF: If modeling double-opponent cells, how are their receptive fields defined? Goal: Generally speaking, what was the purpose of the modeling effort?						

C. Summary

We define single-opponent neurons to possess classical center/surround receptive fields for processing cone input into opponent colors. We define double-opponent neurons to be spatially opposed combinations of single-opponent neurons. We recognize both achromatic and chromatic flavors of these cells, explaining the three axes of the opponent colorspace. By these definitions, we expect single-opponent neurons to respond best to fill field stimulation while double-opponent neurons fire only at boundaries. This understanding treats color and shape as intrinsically connected and, as a consequence, predicts perceptual phenomena such as color induction to arise very early in visual processing.

In the *Method* section which follows, we describe two means by which we incorporate a biologically plausible descriptor of opponent color information into a neurodynamical model. Further still, we extend the model developed by Penacchio *et*

al. [12] to include logical interactions between single-opponent and double-opponent neurons of individual specificities; color, orientation, and spatial frequency.

III. METHOD

We present a computational model designed to be representative of the aforementioned biology. The implementation of this model can be conceived of as two distinct parts:

- *Description of Visual Information*: transformation of image(s) into a biologically meaningful representation.
- *Neurodynamical Processing*: iterative processing of the dynamic interactions between the neurons modeled.

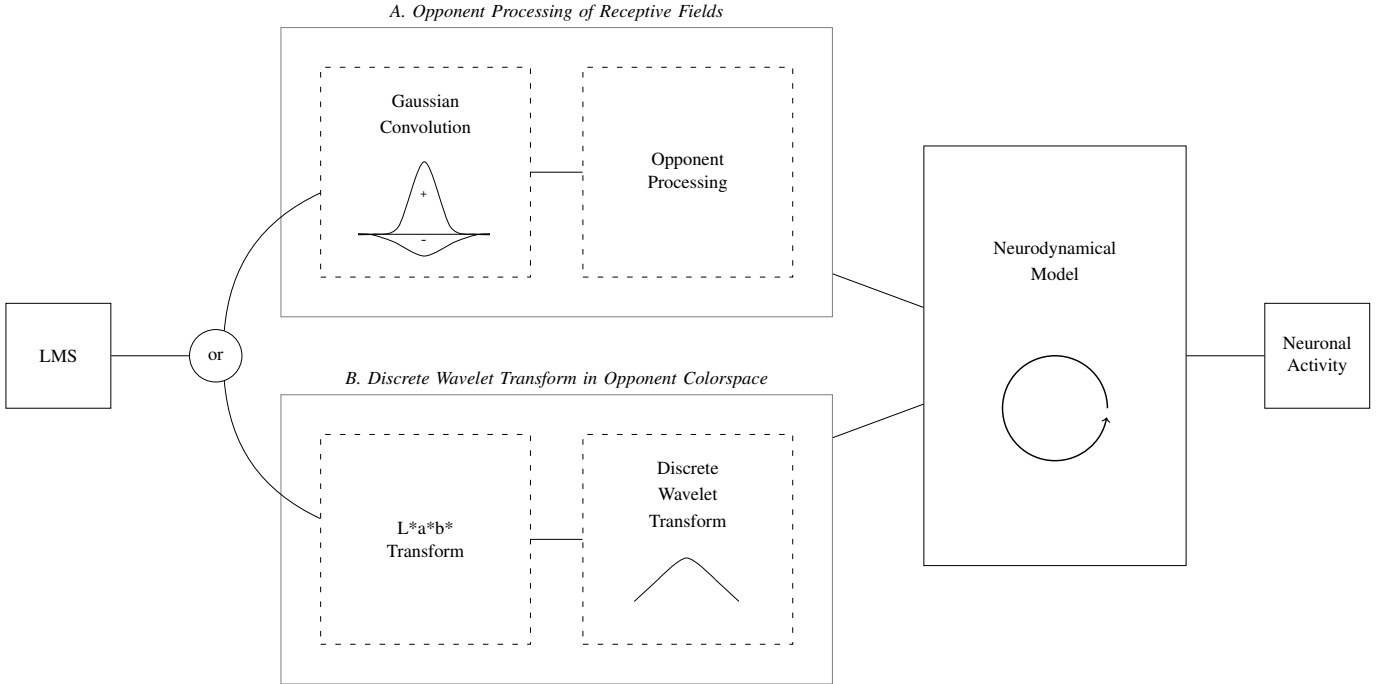


Figure 8: Workflow diagram of algorithm at its highest level. Data can be processed through either *A. Opponent Processing of Receptive Fields* or *Discrete Wavelet Transform in Opponent Colorspace*. This is then fed into the neurodynamical model which outputs a map of neuronal activity.

Description of Visual Information

In accordance with the understanding of biology presented, we propose that a biologically plausible color descriptor should 1) separate opponent color components from each other, and 2) separate surface information from boundary information. We describe two different approaches to this end. The first approach, herein referred to in proximity as the *Opponent Processing of Neural Receptive Fields* method, represents an effort to explicitly transform raw visual data in strict accordance with neurobiological theory. Essentially attempting to mimic the information processing pathways of the retina, lateral geniculate nucleus (LGN), and striate cortex (V1). The second approach, termed with equal verbosity, is the *Discrete Wavelet Transform in Opponent Colorspace* method. Here we stray from the details of the biological pathways in an attempt to achieve the same end, through more computationally efficient means.

In both, the input is a normal RGB image, and the output to the neurodynamical model is a 5 dimensional matrix containing 6 opponent color channels (*Light, Dark, Red, Green, Blue, & Yellow*), each decomposed into its surface and oriented edge components, at 1 or more scales. In this work we consider just 3 directions of orientation preference at edges: horizontal, diagonal, & vertical. Before processing by the neurodynamical model, this data is normalized so as to circumvent differences between the data output by these two methods. This normalization step is described in more detail in the section on *Neurodynamical Processing*.

A. Opponent Processing of Neural Receptive Fields

Processing starts by convolving each of the L, M, and S cone spectral response functions with two different gaussian filters. These convolutions simulate integration of information in a neuron's receptive field. One convolution is used to build the center receptive field, the other convolution, the surround.

Single-opponent cells' receptive fields are the classical center-surround configuration: symmetric, centered, circular gaussians. Typically, the center is smaller and weighed significantly more heavily than the surround, as in Figure 2c. Double-opponent receptive fields are markedly more complex: asymmetrical, off-center, elongated gaussian filters. Similarly, these filters can be adjusted to different sizes, shapes, and weights. For our tests we worked with symmetric balanced receptive fields, as in Figure 5c.

To construct opponent color channels, we contrast center (c) and surround (s) convolutions of the L, M, and S channels into three pairs: two color and one achromatic.

$$\text{Light}(c, s, \sigma) = \max(0, (\frac{L(c, \sigma) + M(c, \sigma)}{2} - 0.5) - (\frac{L(s, \sigma) + M(s, \sigma)}{2} - 0.5)) \quad (24)$$

$$\text{Dark}(c, s, \sigma) = \max(0, (\frac{L(s, \sigma) + M(s, \sigma)}{2} - 0.5) - (\frac{L(c, \sigma) + M(c, \sigma)}{2} - 0.5)) \quad (25)$$

$$\text{Red}(c, s, \sigma) = \max(0, L(c, \sigma) - M(s, \sigma)) \quad (26)$$

$$\text{Green}(c, s, \sigma) = \max(0, M(c, \sigma) - L(s, \sigma)) \quad (27)$$

$$\text{Blue}(c, s, \sigma) = \max(0, S(c, \sigma) - \frac{L(s, \sigma) + M(s, \sigma)}{2}) \quad (28)$$

$$\text{Yellow}(c, s, \sigma) = \max(0, \frac{L(c, \sigma) + M(c, \sigma)}{2} - S(s, \sigma)) \quad (29)$$

A schematic of this workflow is presented in Figure 9. It is clear from this schematic, and the equations above, that L and M input are significantly overrepresented. This reflects the biological overrepresentation of the evolutionarily older L and M pathways in human vision, and is more in line with, say, work by Spitzer *et al.* [22] than Itti *et al.* [5]. Our equations for Light and Dark, however, are novel.

Because the inputs to the Light and Dark receptive fields come from the same cones (L and M), classical opponent center/surround receptive fields will not function to capture both Light and Dark. This can be easily seen in Figure 9; while the Light, Red, Green, Blue, and Yellow all have *on* centers and *off* surrounds, Dark has an *on* surround and an *off* center. This is supported by literature [15] but introduces issues. For example, by having Light and Dark activity be almost completely complementary, we find double-opponent activity in these channels to be almost completely redundant, as can be seen in the Appendix, Figure 22.

Double-opponent cells' responses constructed along the same workflow as single-opponent cells', though their receptive fields are different, Figure 10. Different responses are obtained for each preferred orientation by convolving the image with oriented receptive fields. In this work we considered only three basic orientations: horizontal, vertical, and diagonal.

In our implementation, for convenience, we utilize the R, G, and B channels of the raw image as an approximation of L, M, and S cone activity, respectively. It should be noted that this is not biologically reasonable and a preprocessing step should be performed to obtain input more representative of L, M, and S cone spectral responses.

Both single and double-opponent responses are obtained at a number of scales, depending on the size of the input image. To achieve this, the size of the gaussian used to convolve the images are increased exponentially by scale. This reflects neurons' spatial frequency selectivity and confers a degree of scale invariance to the model.

To summarize, this first of two approaches to color description aims to be true to the biology at all cost. We explicitly model the receptive fields of both single-opponent and double-opponent neurons. These receptive fields are used to transduce retinal activity of L, M, and S cones into the cell activity expected in V1. By defining the receptive fields explicitly, we obtain a large degree of control over the response patterns. However, biologically meaningful tuning of these parameters may be impossible given the current understanding of cells' receptive fields. Finally, it is worth noting that this approach involves a large number of convolutions and proves to be relatively slow; orders of magnitude slower than the next approach we will present. This performance penalty, however, is a one time cost as the input is prepared, it does not affect the performance of the neurodynamical model in any way.

B. Discrete Wavelet Transform in Opponent Colorspace

Previous work by Penacchio *et al.* [12] utilized a discrete wavelet transform (DWT) to decompose a greyscale image into its oriented edge components, at scales. In the context of our current research, this could be thought of as representing achromatic double-opponent cells; the response is greatest at luminance boundaries and nonexistent on surfaces or at chromatic changes. In this work we extend their approach to the opponent colorspace and examine its applicability as a replacement of the previously detailed *Opponent Processing of Neural Receptive Fields*.

Unlike the previously presented color descriptor, this transformation begins not with the convolution step, but instead with a colorspace transformation. We convert the image from RGB to CIE $L^*a^*b^*$. This colorspace separates luminance from its two opponent color channels. The two color channels are 0 centered; with positive and negative values in a^* denoting redness and greenness, respectively, while positive and negative values in the b^* channel indicate blueness and yellowness, respectively.



Figure 9: Diagram of *Opponent Processing of Neural Receptive Fields* workflow. The L, M, and S channels are convolved with center and surround gaussians and then combined to build opponent colors, here exemplified by single-opponent cell receptive fields. The process is similar for double-opponent cells.

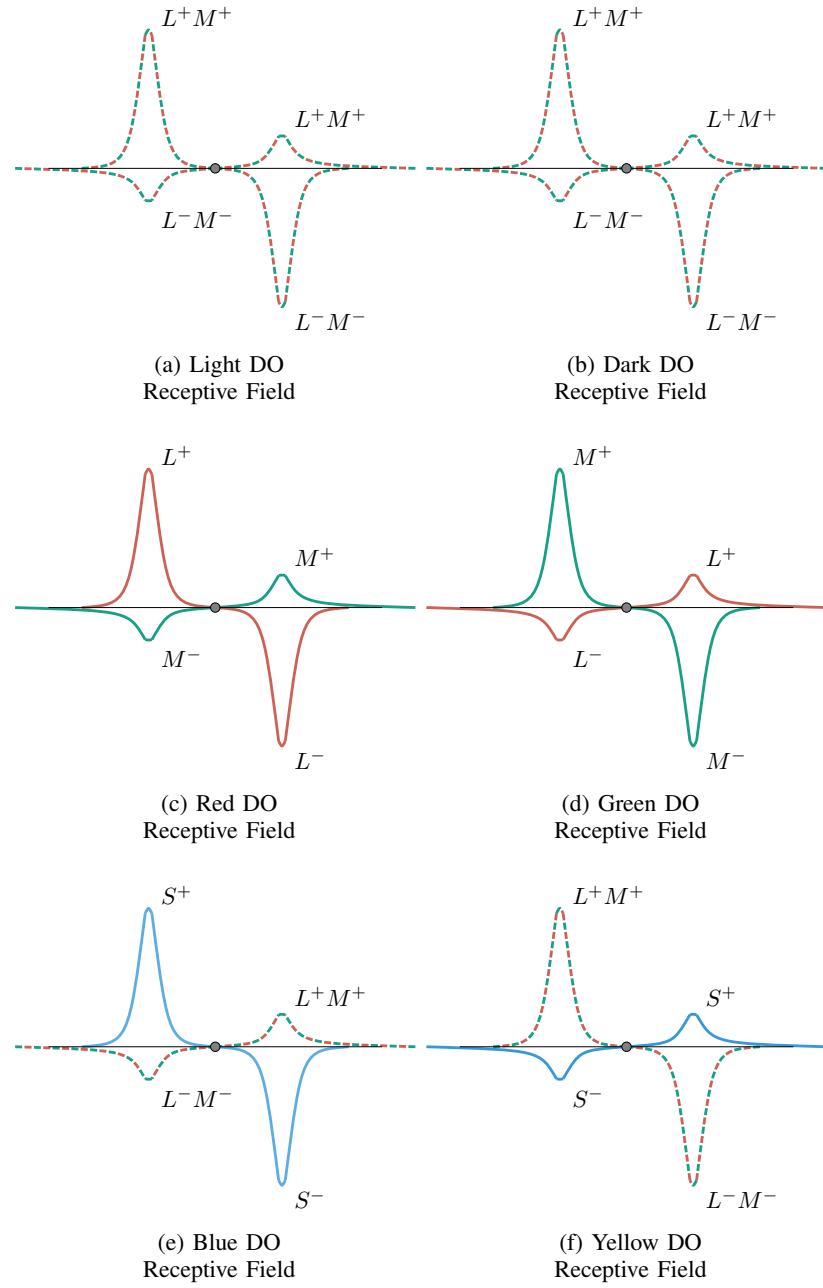
Figure 10: Double-opponent receptive fields utilized in *Opponent Processing of Neural Receptive Fields*.



Figure 11: Schematic of orientation selectivity in double-opponent receptive field configurations.

The luminance channel, L^* , scales from 0 to 100, 0 being total darkness, 100 being pure brightness. We subtract 50 from this channel to obtain a 0 centered range of luminance. We consider positive values to define lightness and negative values darkness.

We then obtain the DWT in this modified *CIE L^{*}a^{*}b^{*}* colorspace. Similar to the gaussian convolutions in the previous method, this transformation can be interpreted as representing processing in a cell's receptive field. That is, the activity of a particular cell is now defined not just by its own activity, but also of the activity of the cells around it.

Following multiresolution and orientation decomposition, all wavelet and residual planes are 0 centered, thus we can easily split them into independent opponent components:

$$\text{Light} = \max(0, L^* - 50) \quad (30)$$

$$\text{Dark} = |\min(0, L^* - 50)| \quad (31)$$

$$\text{Red} = \max(0, a^*) \quad (32)$$

$$\text{Green} = |\min(0, a^*)| \quad (33)$$

$$\text{Blue} = \max(0, b^*) \quad (34)$$

$$\text{Yellow} = |\min(0, b^*)| \quad (35)$$

The result of this process can be seen in the Appendix, Figure 23.

Neurodynamical Processing

Stage I of the proposed method focuses on the description of color in a biologically meaningful form, of which we've described two distinct approaches. Stage II is to further process this data in an iterative computational model of neurodynamical processes, as defined in Equations 36 and 37. The input stimulus, from Stage I, at time τ , $I_{i\gamma\sigma\theta}^\tau$ drives the model and mainly determines its response. The normalization of the stimulus at each time step is extended from that proposed by Li [9] and Penacchio [12]. We normalize within each color channel (γ), scale (σ), and orientation (θ). At the first time step, $I_{i\gamma\sigma\theta}^1$ is used to bootstrap the model and set as the initial excitation response, $x_{i\gamma\sigma\theta}$.

$x_{i\gamma\sigma\theta}$ can be viewed as a model of retinotopic excitation hypercolumns in V1, with i specifying the retinally mapped location of the hypercolumn. Similarly, $y_{i\gamma\sigma\theta}$ may be interpreted as its retinotopic inhibitory counterpart. $\dot{x}_{i\gamma\sigma\theta}$ and $\dot{y}_{i\gamma\sigma\theta}$, then, are the change in excitatory and inhibitory membrane potentials over time, respectively, and follow the equations:

$$\begin{aligned} \dot{x}_{i\gamma\sigma\theta} = & -\alpha_x x_{i\gamma\sigma\theta} \\ & - g_y(y_{i\gamma\sigma\theta}) \\ & - \sum_{\gamma' \neq \text{opp}(\gamma), \Delta_\sigma, \Delta_\theta \neq 0} \Psi(\gamma', \Delta_\sigma, \Delta_\theta) g_y(y_{i\gamma\sigma+\Delta_\sigma\theta+\Delta_\theta}) + J_0 g_x(x_{i\gamma\sigma\theta}) \\ & + \sum_{j \neq i, \gamma' \neq \text{opp}(\gamma), \sigma' \theta'} J_{[i\gamma\sigma\theta, j\gamma'\sigma'\theta']} g_x(x_{j\gamma'\sigma'\theta'}) \\ & + I_{i\gamma\sigma\theta}^\tau \\ & + I_0 \end{aligned} \quad (36)$$

$$\begin{aligned} \dot{y}_{i\gamma\sigma\theta} = & -\alpha_y Y_{i\gamma\sigma\theta} \\ & + g_x(X_{i\gamma\sigma\theta}) \\ & + \sum_{j \neq i, \gamma' \sigma' \theta'} W_{[i\gamma\sigma\theta, j\gamma'\sigma'\theta']} g_x(x_{j\gamma'\sigma'\theta'}) \\ & + I_c \end{aligned} \quad (37)$$

where $\alpha_x x_{i\gamma\sigma\theta}$ and $\alpha_y Y_{i\gamma\sigma\theta}$ model the decay to the resting potential, $g_x(x)$ and $g_y(y)$ are sigmoid-like functions modeling cells' firing rates in response to membrane potentials x and y , respectively, $\Psi(\gamma', \Delta_\sigma, \Delta_\theta) \leq 1$ is the spread of inhibition within a hypercolumn, $J_0 g_x(x_{i\gamma\sigma\theta})$ is self-excitation, and I_c is background noise [9]. Any cell can interact with another by exciting it or inhibiting it, via monosynaptic excitation through excitatory-excitatory horizontal connections, or disynaptic inhibition through excitatory-inhibitory connections, respectively [12]. Such interactions are modeled between cells within and across hypercolumns; color, scale, and orientation, as well as between cells within and across cell classes; double-opponent and single-opponent. These cellular interactions are defined by $J_{[i\gamma\sigma\theta, j\gamma'\sigma'\theta']}$ (excitatory) and $W_{[i\gamma\sigma\theta, j\gamma'\sigma'\theta']}$ (inhibitory).

Orientation (θ): The excitatory and inhibitory interactions between orientation specific double-opponent cells are exactly as those defined by Penacchio [12] and Li [9]. Single-opponent cells, introduced in our work, are non-directional; they have no preferred orientation θ . $\Delta\theta$ is thus not computable and so this class of cells do not inhibit the activity of other cells. Single-opponent cells do not contribute to W . In order to explore 'fill in' effects, however, we support parameterization of excitatory weights to and from single-opponent and double-opponent cells. This weight functions as $\Delta\theta$ and is equal for all preferred orientations of the double-opponent cells. These interactions are modeled by a circular-symmetric gaussian in J .

Scale (σ): As in Penacchio [12], we decompose the input signal into signal at different scales. This reflects single-opponent and double-opponent cells' spatial frequency selectivity derived from their receptive fields. While this confers a level of scale invariance to the model, the primate visual cortex is not completely scale invariant and nor should our model be. Both image transformation methods presented in Stage I inherently represent activity at lower spatial frequencies with higher response.

Color (γ): We introduce a novel concept to the neurodynamical model framework developed by Li [9] and Penacchio [12]: color. Unfortunately, the structural organization of color preferring cells and the connections between them is not well understood and leading theories are still quite controversial [18]. We herein define a set of *logical* rules of interaction opponent color cells (including achromatic cells).

If a cell is stimulated, it excites nearby cells of the same orientation and scale preference, in any color channel other than its opponent. Conversely, a stimulated cell will inhibit nearby cells of the same orientation and scale preference, only in its opponent color channel. For example, stimulation of a DO cell preferring 'yellow' vertical edges will excite a DO cell preferring 'red' vertical edges at the same location. It will equally excite 'green', 'light', and 'dark' cells preferring the same orientation in the same location. It will not, however, excite cells of its opponent color 'blue'. In fact, it will inhibit activity in 'blue' cells preferring this same orientation in the same location.

We propose that these rules of interaction are logical as only opponent colors are mutually exclusive. While a bluish yellow line is not permissible in the opponent colorspace, a bluish green, bluish red, bright blue, or dark blue line is entirely plausible. Each of the possible combinations are equally probable and so the excitatory-excitatory connections between cells of these color preferences are equally weighed. These excitatory and inhibitory rules are encoded in J and W , respectively.

Activity Normalization (I_0): The general and local normalization of activities [4] has been extended from its use by Li [9] and Penacchio [12]. We normalize excitatory membrane potentials within double-opponent cells of similar location (i), color (γ), scale (σ), and orientation (θ) preferences. Likewise we normalize single-opponent cells of similar location (i), color (γ), scale (σ). We found it important to normalize the activity of these two classes of neurons independently as the information encoded by each is radically different: localized edge information by double-opponent cells, and extensive surface information by single-opponent cells.

IV. EXPERIMENTS

We evaluated the performance of our model by applying it to a number of test images seen to exhibit color induction effects. The expectation was that the model predict the perceived phenomena. All experiments involved two or more test stimuli in which human observers can describe a difference between them that doesn't physically exist. For example, most would describe the left inner ring in Figure 1 as being green and the right inner ring as being blue. As is shown, however, the two rings are physically identical. We would expect our model to predict this effect by displaying different neural activity at these two locations.

For each test image, we applied both the *Opponent Processing of Neural Receptive Fields* and *Discrete Wavelet Transform in Opponent Colorspace* methods so as to compare their performance. In both cases, the output of the model was the retinotopic neural activity in each of the opponent channels. For each test image, we compared this output for differences in *direction* and *magnitude* of activity. For example, in Figure 1 we would expect to see activity in the Red-Green channel toward green for the left inner ring, and Blue-Yellow activity toward blue for the right inner ring.

All experiments were run with the same model configurations, except where inapplicable, e.g., double-opponent receptive field gaussian configurations are unique to the *Opponent Processing of Neural Receptive Fields* method. All experiments were run for 20 membrane time steps of the neurodynamical model (τ), each time step involving 10 iterations of neural interactions. The output was taken from each time step, excluding the first bootstrapping step, and averaged to obtain a single view of the neural activity in each color channel during the whole experiment. The 3 pairs of opponent colors were subtracted from each other to obtain 3 opponent color channels: Light-Dark, Red-Green, and Blue-Yellow.

These opponent color channels no longer reside in any known colorspace. Even in the cases where we used the *CIE L*a*b** colorspace transform as input, the output is a measure of neural activity; it is on a completely different scale. As such, the output color channels are visualized independently and interpreted to contain the expected response or not. In all, whiter values indicate activity toward the positive pole, e.g., Red in Red-Green, while darker values indicate activity toward the negative pole, e.g., Green in Red-Green. For each experiment, all output images are on the same scale. However, the scale of results *between* experiments is not consistent; results cannot be compared across experiments.

In some experiments, the differences between test stimuli responses were subtle relative to other activities in the population. To help visually observe differences in activity at the locations it was expected, we masked all other regions of the output and rescaled the visual representation. Still, whiter values indicate activity toward the positive pole and darker values activity toward the negative pole. However, in some cases rescaling enhances differences otherwise missed. Again, all enhanced images in each experiment are on the same scale and can be compared, but enhanced results from experiments are on individual scales and thus cannot be compared.

V. RESULTS

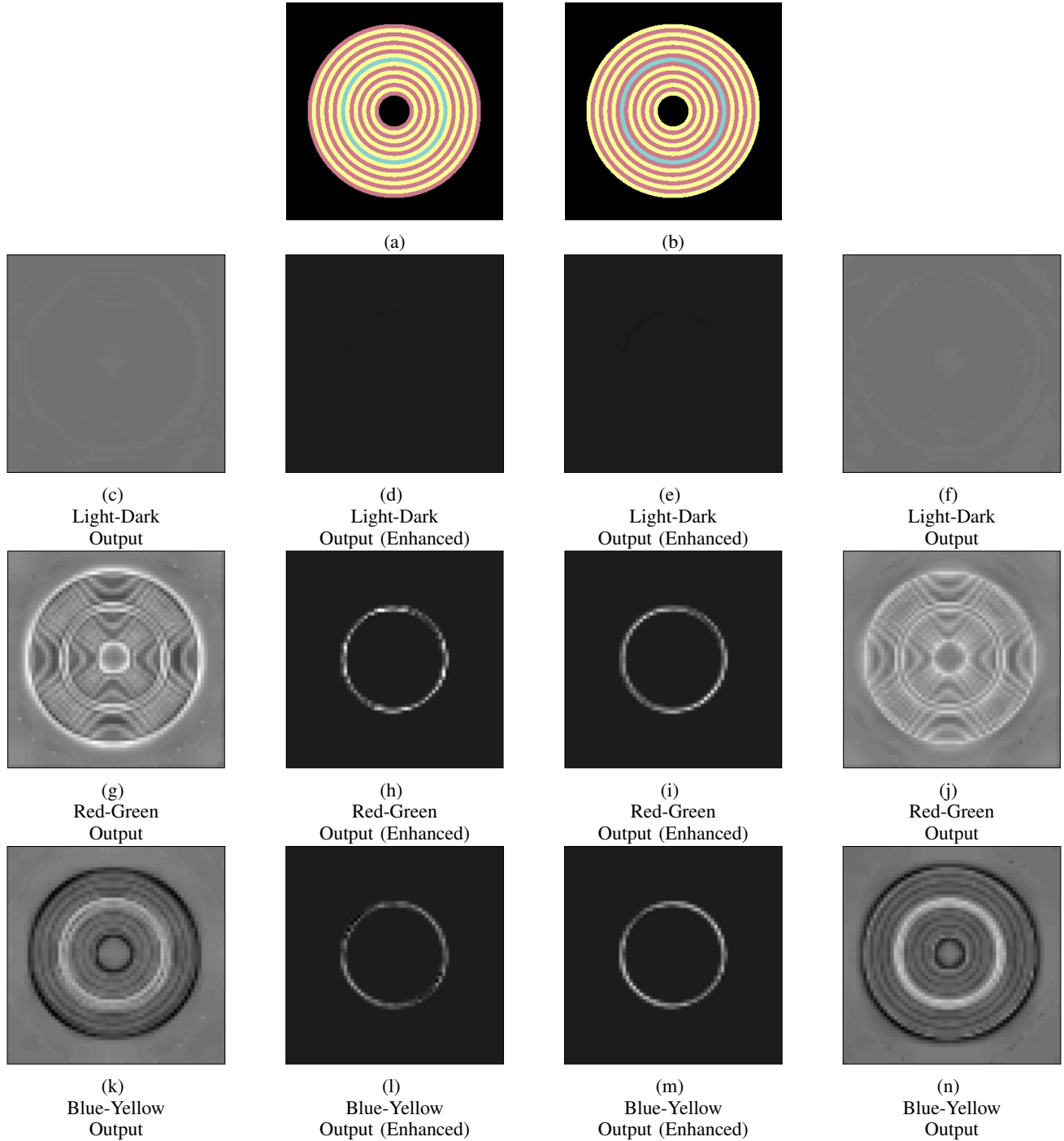


Figure 12: Experimental results for the given test stimuli, 12a & 12b, processed by the *Opponent Processing of Neural Receptive Fields* method. In 12c, 12g, and 12k we have the raw output of the L-D, R-G, and B-Y channels for the *left* stimulus (which appears green). In 12f, 12j, and 12n we have the raw output of the L-D, R-G, and B-Y channels for the *right* stimulus (which appears blue). In 12d, 12h, and 12l we mask the raw output of the *left* stimulus so as to isolate the test ring. In 12e, 12i, and 12m we mask the raw output of the *left* stimulus so as to isolate the test ring.

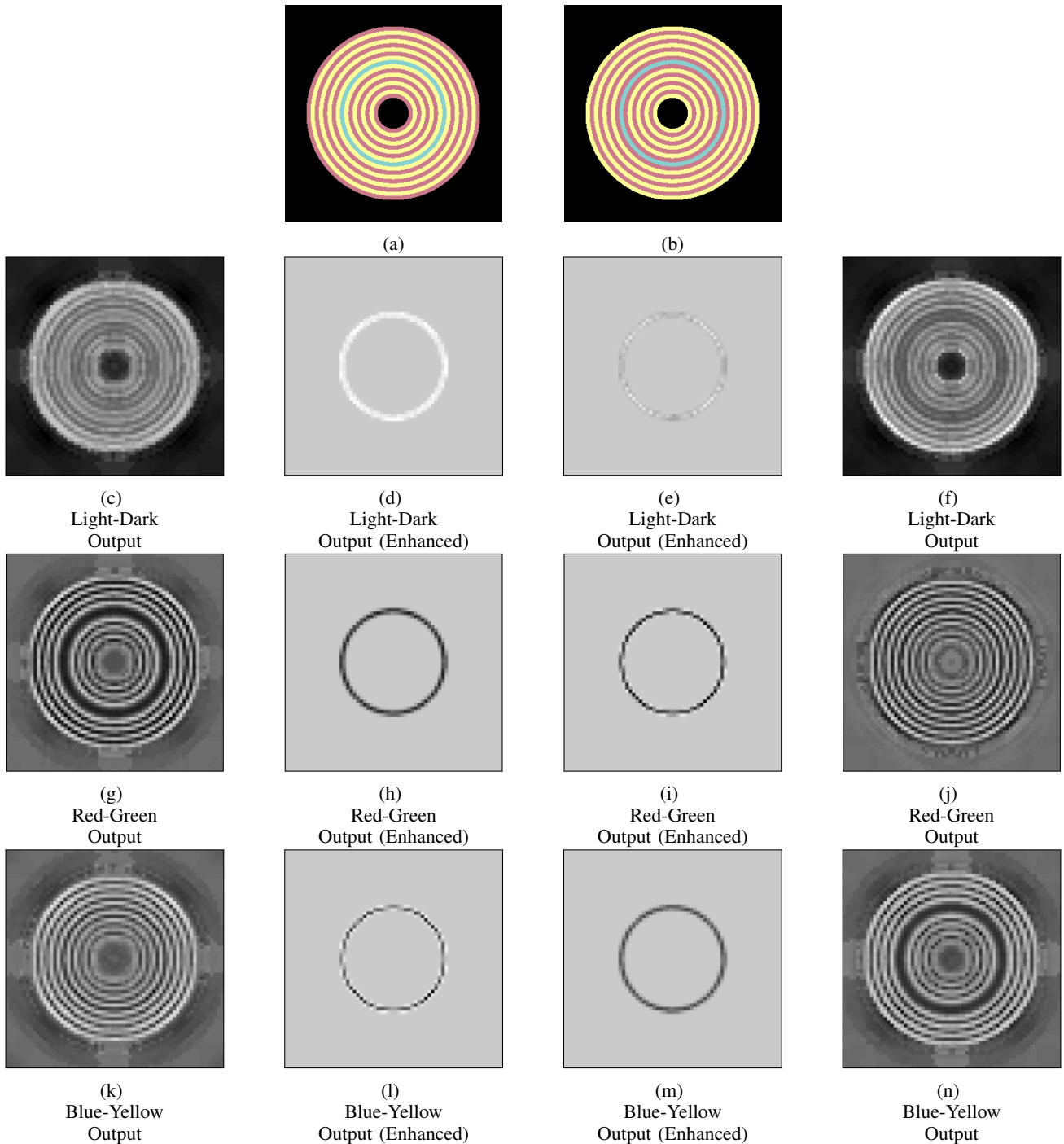


Figure 13: Experimental results for the given test stimuli, 13a & 13b, processed by the *Discrete Wavelet Transform in Opponent Colorspace* method. In 13c, 13g, and 13k we have the raw output of the L-D, R-G, and B-Y channels for the *left* stimulus (which appears green). In 13f, 13j, and 13n we have the raw output of the L-D, R-G, and B-Y channels for the *right* stimulus (which appears blue). In 13d, 13h, and 13l we mask the raw output of the *left* stimulus so as to isolate the test ring. In 13e, 13i, and 13m we mask the raw output of the *left* stimulus so as to isolate the test ring.

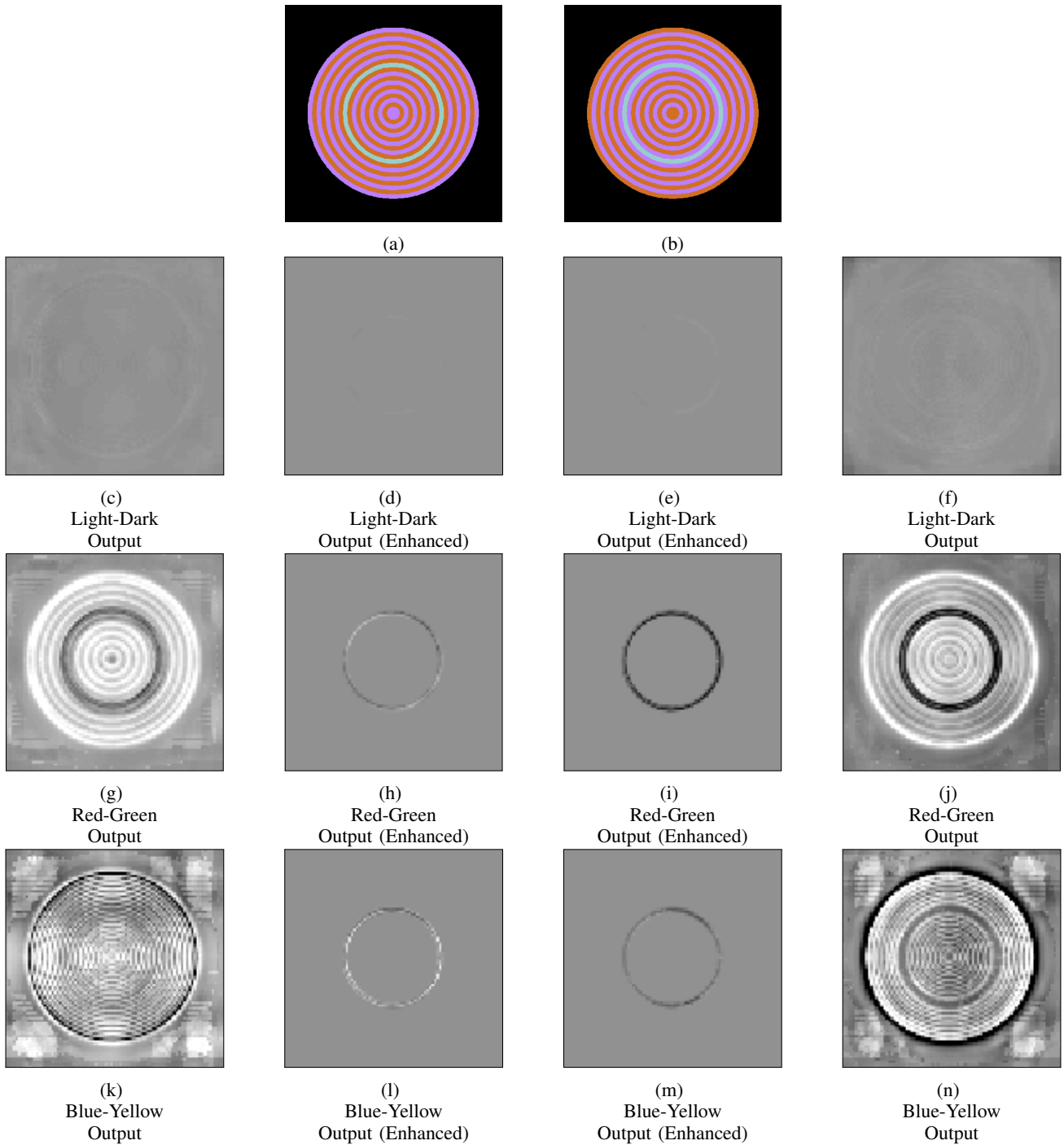


Figure 14: Experimental results for the given test stimuli, 14a & 14b, processed by the *Opponent Processing of Neural Receptive Fields* method. In 14c, 14g, and 14k we have the raw output of the L-D, R-G, and B-Y channels for the *left* stimulus (which appears green). In 14f, 14j, and 14n we have the raw output of the L-D, R-G, and B-Y channels for the *right* stimulus (which appears blue). In 14d, 14h, and 14l we mask the raw output of the *left* stimulus so as to isolate the test ring. In 14e, 14i, and 14m we mask the raw output of the *left* stimulus so as to isolate the test ring.

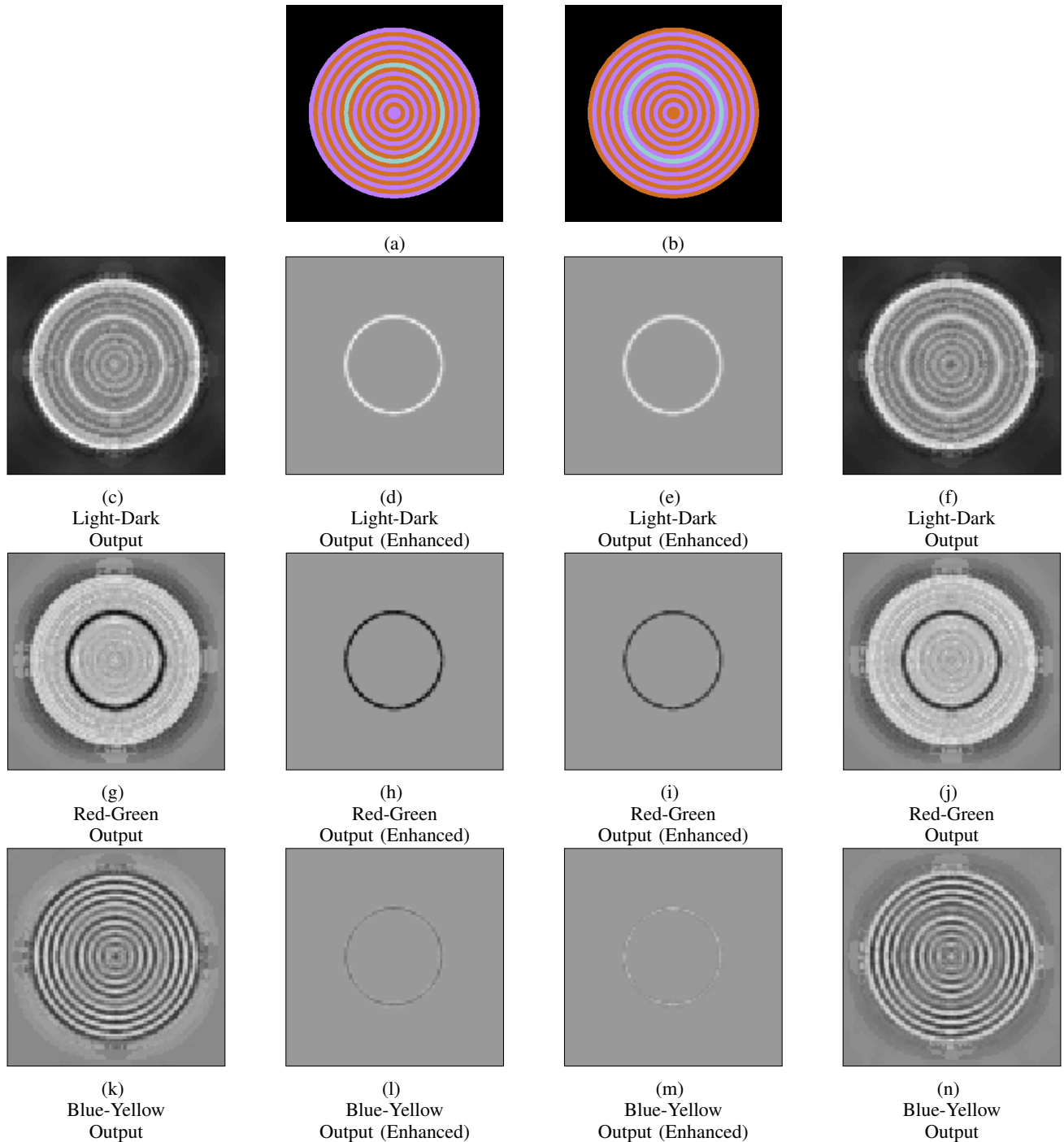


Figure 15: Experimental results for the given test stimuli, 15a & 15b, processed by the *Discrete Wavelet Transform in Opponent Colorspace* method. In 15c, 15g, and 15k we have the raw output of the L-D, R-G, and B-Y channels for the *left* stimulus (which appears green). In 15f, 15j, and 15n we have the raw output of the L-D, R-G, and B-Y channels for the *right* stimulus (which appears blue). In 15d, 15h, and 15l we mask the raw output of the *left* stimulus so as to isolate the test ring. In 15e, 15i, and 15m we mask the raw output of the *left* stimulus so as to isolate the test ring.

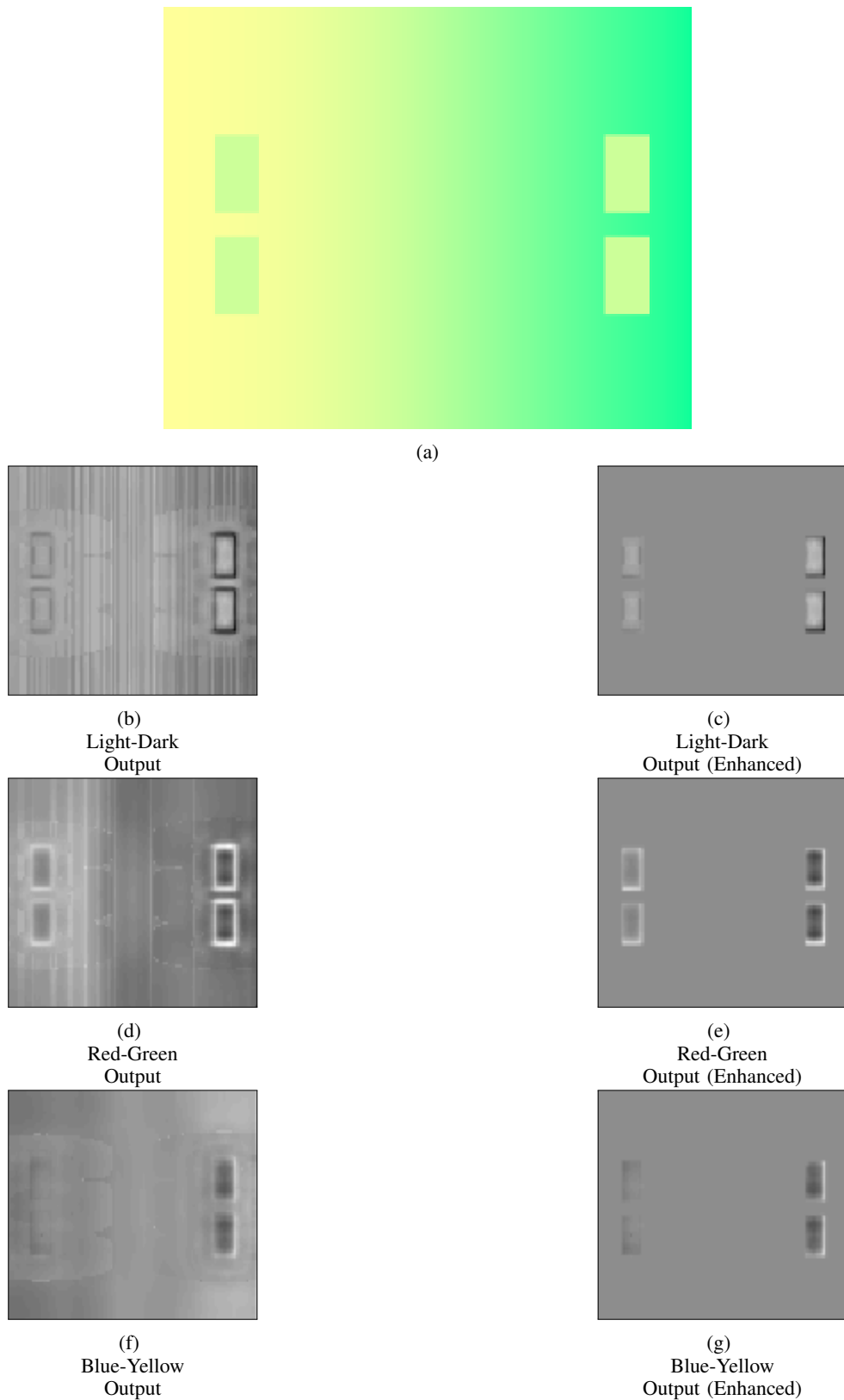


Figure 16: Experimental results for the given test stimuli, 16a, processed by the *Opponent Processing of Neural Receptive Fields* method. In 16b, 16d, and 16f we have the raw output of the L-D, R-G, and B-Y channels. In 16c, 16e, and 16g we mask the raw output so as to isolate and enhance the test patches.

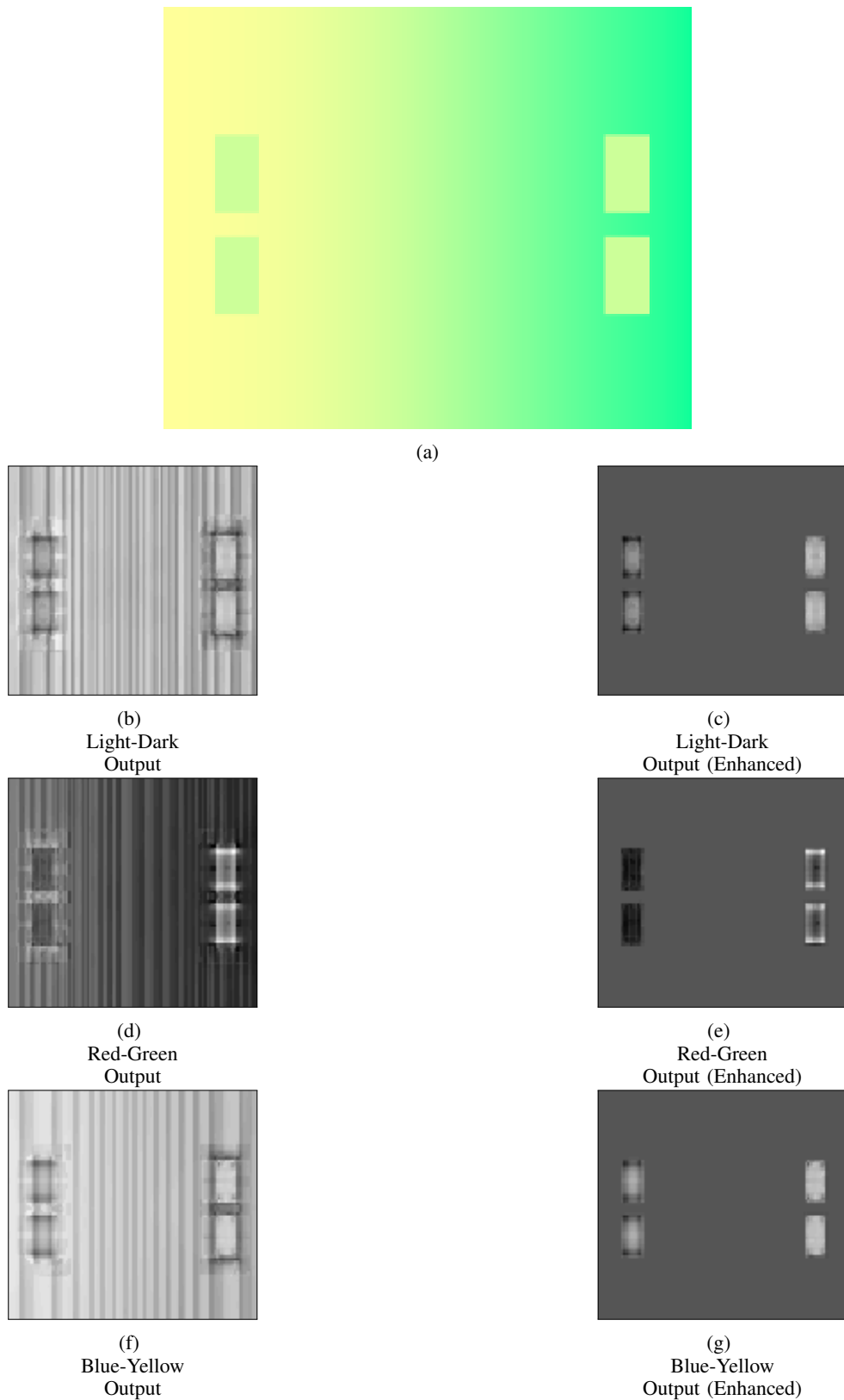


Figure 17: Experimental results for the given test stimuli, 17a, processed by the *Discrete Wavelet Transform in Opponent Colorspace* method. In 17b, 17d, and 17f we have the raw output of the L-D, R-G, and B-Y channels. In 17c, 17e, and 17g we mask the raw output so as to isolate and enhance the test patches.

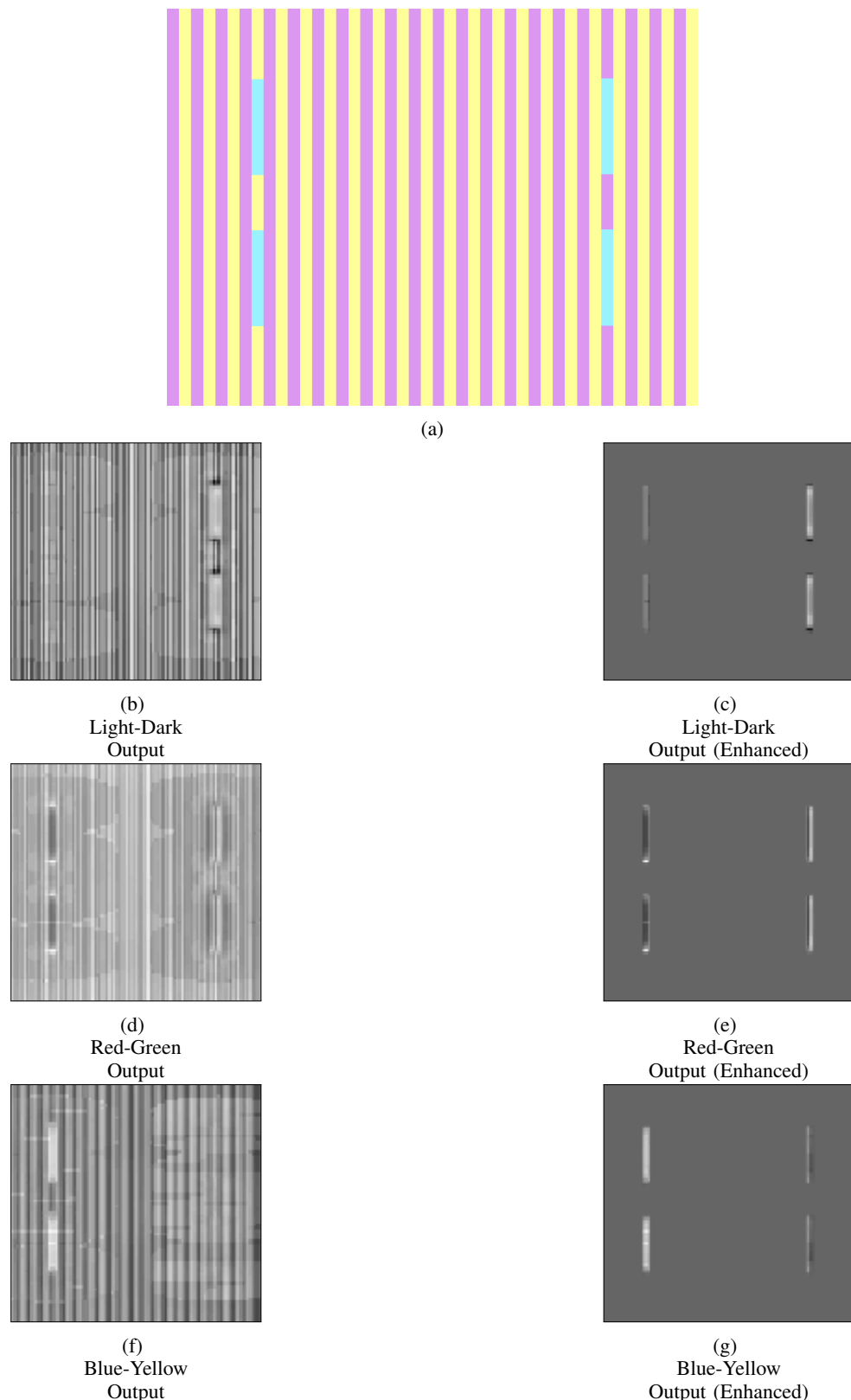


Figure 18: Experimental results for the given test stimuli, 18a, processed by the *Opponent Processing of Neural Receptive Fields* method. In 18b, 18d, and 18f we have the raw output of the L-D, R-G, and B-Y channels. In 18c, 18e, and 18g we mask the raw output so as to isolate and enhance the test patches.

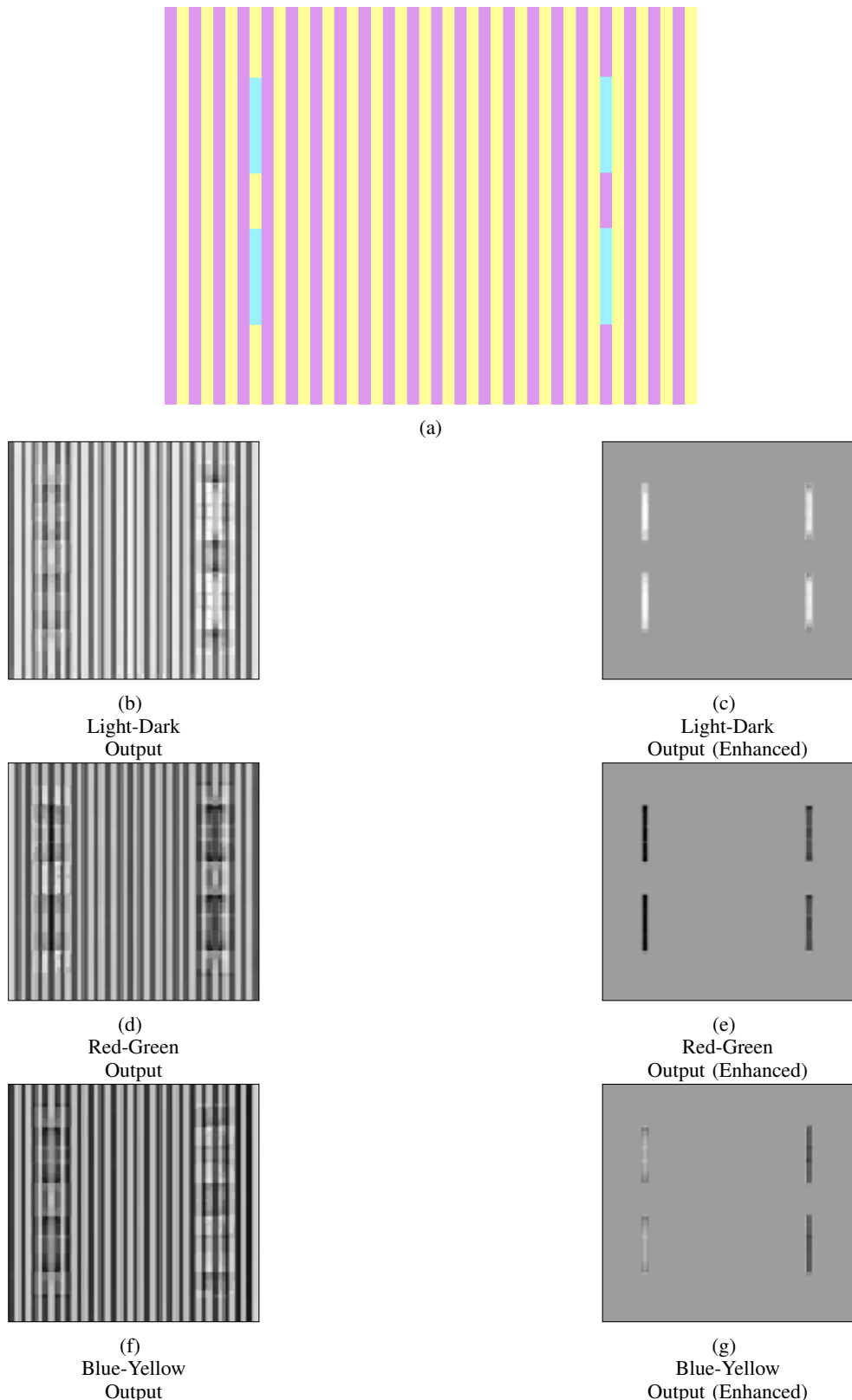


Figure 19: Experimental results for the given test stimuli, 19a, processed by the *Discrete Wavelet Transform in Opponent Colorspace* method. In 19b, 19d, and 19f we have the raw output of the L-D, R-G, and B-Y channels. In 19c, 19e, and 19g we mask the raw output so as to isolate and enhance the test patches.

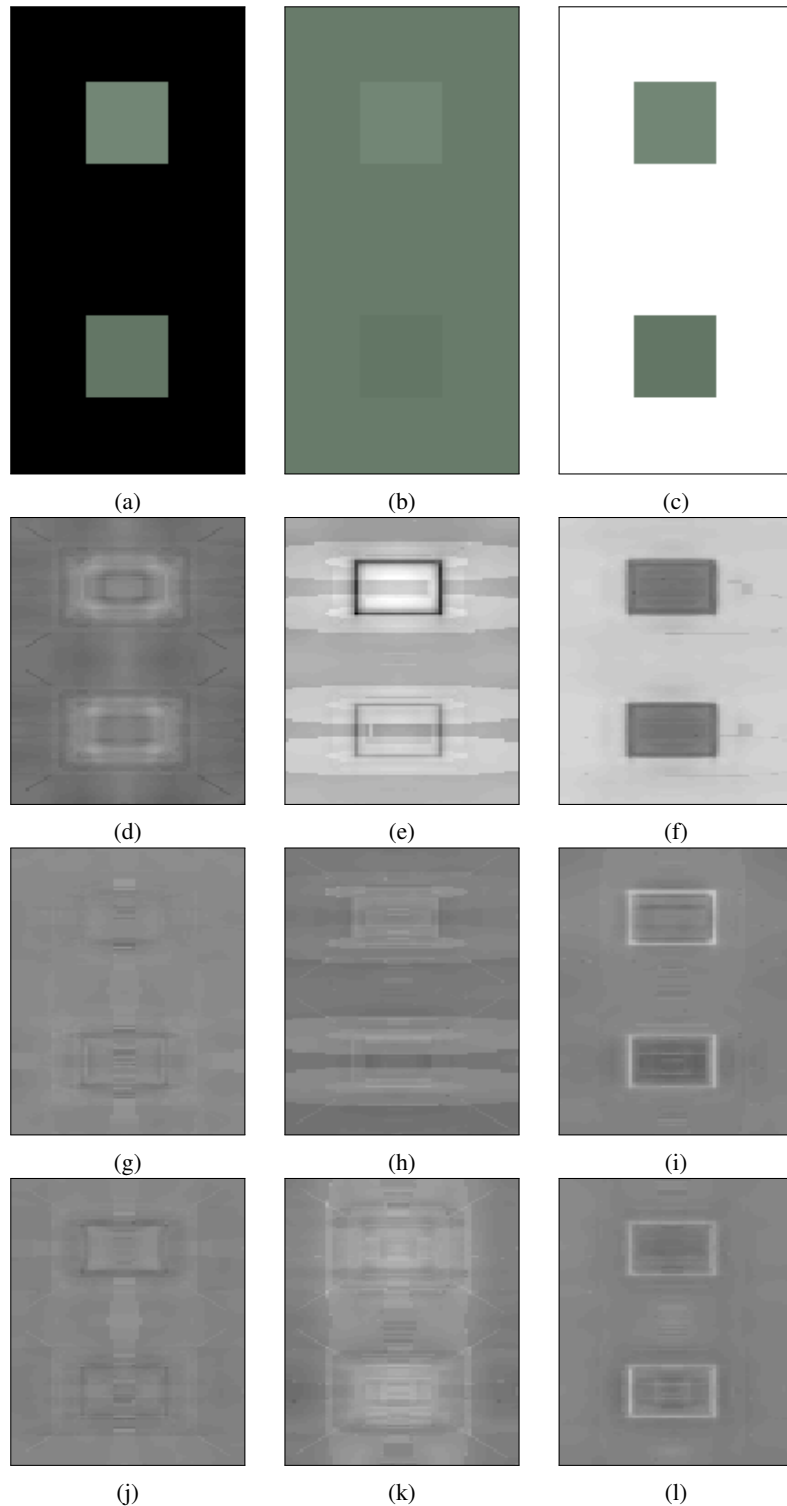


Figure 20: Experimental results for the given test stimuli, processed by the *Opponent Processing of Neural Receptive Fields* method. Perceptually, humans find it difficult to distinguish the upper and lower boxes, which differ in brightness only slightly, when presented on a luminous background like black or white. However, it is easy to distinguish them on a background whose luminance lies between them. We obtain positive results in Figure 20e which identify a luminance difference between the two squares.

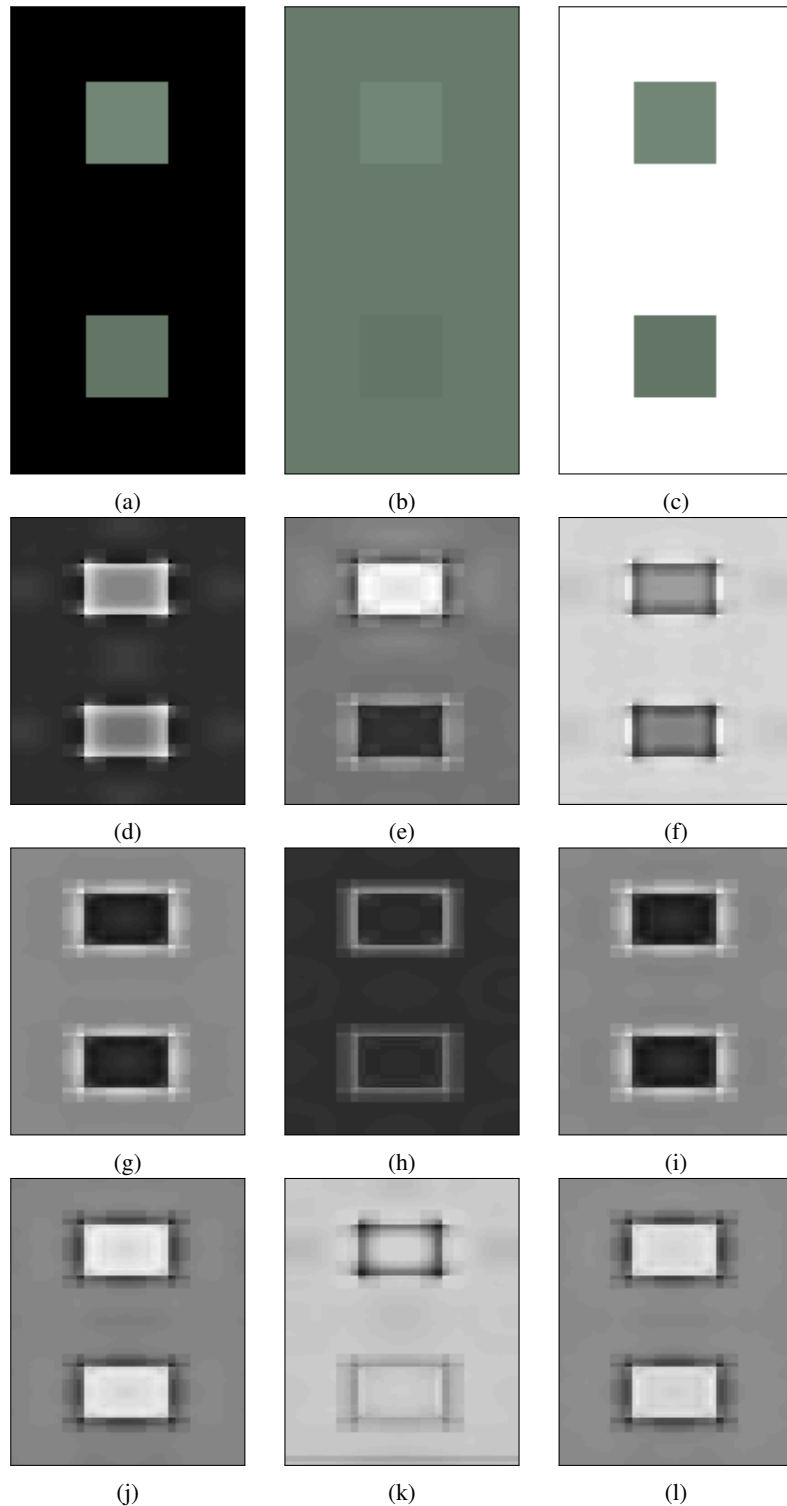


Figure 21: Experimental results for the given test stimuli, processed by the *Discrete Wavelet Transform in Opponent Color space* method. Perceptually, humans find it difficult to distinguish the upper and lower boxes, which differ in brightness only slightly, when presented on a luminous background like black or white. However, it is easy to distinguish them on a background whose luminance lies between them. We obtain positive results in Figure 21e which identify a luminance difference between the two squares.

VI. CONCLUSIONS

We have presented our work on the introduction of a biologically plausible representation of color into a neurodynamical model of V1. To do so we included models of single-opponent and double-opponent cell response patterns, and the interactions between such cells, to the neurodynamical model developed by Penacchio *et al.* The neuronal interactions were defined logically, as little biological evidence exists to describe their physical interactions. With respect to modeling the cells' responses, we explored two different approaches:

1) *Opponent Processing of Neural Receptive Fields*: This was an attempt to adhere to what is reported in neurobiology. This approach is conceptually very enticing due to its biological plausibility. However, our implementation proved to be relatively slow: orders of magnitude slower than our second approach. This can likely be improved by 1) reusing convolutions performed at the single-opponent level to build double-opponent receptive fields, or 2) utilizing Gabor filters rather than gaussians to convolve the input. In general, we found this approach to not be as sensitive to detail as the *Discrete Wavelet Transform in Opponent Space*, in Figure 12 for example. We suspect this is can be easily addressed by more attentive tuning of the algorithm's parameters, specifically, gaussian receptive field configurations at higher scales. We also run into a significant issue in how we mathematically defined the Light and Dark opponent color components (Eqs. 24 & 25). Unlike their chromatic counterparts, these channels are almost exactly *complementary*. This leads to *redundancy* at the double-opponent level, as can be clearly seen in their receptive field diagrams (Figures 10a & 10b). This is also evident in the redundancy of their response patterns in Appendix Figure 22. This leads to inhibition between the two opponents and they eventually cancel out, as we see in our results, e.g., Figures 12c & 12f. The solution here may also just be a matter of defining appropriately sizes and weights for the cells' receptive fields, or it may require we return to the literature to develop a better understanding of the biology, and a new mathematical model for it.

2) *Discrete Wavelet Transform in Opponent Colorspace*: This color descriptor aimed to be much more computationally efficient, though it sacrificed biologically plausibility along the way. We maintain two key points of contention with the concepts behind this approach. First, as we implemented it, it depends on the *CIE L*a*b** opponent colorspace which was designed to represent color in a perceptually uniform manner. However, this is not to say that it represents color in a biologically meaningful manner. Replacing this colorspace transformation with another may well satisfy these reservations. The other issue with this approach, however, is not so easily addressed. The decomposition of image data, be it through a discrete wavelet transform (DWT) or any other method of convolution, after an explicit mathematical colorspace transformation, be it *CIE L*a*b** or any other, does not reflect the biological order of operations. In the *Opponent Processing of Neural Receptive Fields* method, we convolve L, M, S input as we transform to the opponent colorspace, while in the *Discrete Wavelet Transform in Opponent Colorspace*, we transform to the opponent colorspace before we convolve the signal. This difference is not insignificant and leads us to favor the former method over the latter, at least in principle.

3) *Neurodynamical Model*: The neurodynamical model used in this research has been shown to explain well some of the biological phenomena believed to emerge in V1, such as saliency [9] and brightness induction [12]. It seems logical that it would continue to explain these and others through the introduction of color. However, for this assumption to hold, it is imperative that color be introduced in a meaningful manner. Beyond the description of color information itself, the connections between the new cells introduced to the model need to be defined appropriately. Unfortunately, as mentioned, we found few specificities in the literature to describe such connections.

Given our descriptions of color information and our implementation of neuronal interactions (albeit more logical than biological) we see that brightness induction does still emerge from the model: Figures 20 & 21. In these experiments we see that there is little, if any, difference between the upper and lower test squares when presented on black or white backgrounds (Figures 20d, 20f, 21d, & 21f). However, when presented on a background whose luminance lies between the two test squares, the model responds differently to the upper and lower square (Figures 20e & 21e). In these experiments, the driving factor is brightness. That is, the most important color components in play are Light and Dark. It is encouraging to see that both approaches to color description pass this test, though the differences in their response patterns warrants further investigation.

When we apply the algorithm with chromatic test cases, the results are less conclusive. In the example we first presented in this paper (Figure 1), we find the *Opponent Processing of Neural Receptive Fields* method to identify no significant difference between the two stimuli (Figure 12), while the *Discrete Wavelet Transform in Opponent Colorspace* method predicts a perceived difference contrary to that expected: the blue stimulus elicits activity toward yellowness (Figure 13m), while the green stimulus elicits activity toward redness (Figure 13h). It is worth noting here that it does correctly predict the green stimulus as brighter than the blue stimulus (Figure 13e); perhaps this is an indication that color and brightness do, in fact, need to be treated differently in such a model.

We see similar results when we apply the algorithm to less appealing, but equally impressive examples of chromatic induction: Figures 14 & 15. Here the *Opponent Processing of Neural Receptive Fields* color descriptor results in a prediction that the blue stimulus elicits activity toward yellowness (Figure 15m), while the green stimulus elicits activity toward redness (Figure 15h). These results would lead this author to consider simply flipping the chromatic axes and being satisfied, however, here we see the *Discrete Wavelet Transform in Opponent Colorspace* method returns the expected output: the blue stimulus elicits activity toward blue (Figure 15n) while the green stimulus elicits activity toward green (Figure 15g). This is encouraging, though the degree of difference between the two stimuli does not appear significant.

We also tested the model on larger scaled chromatic induction effects so as to rule out issues with low spatial frequency responses. In Figures 16a and 17a we test the two color descriptors on a green-yellow gradient chromatic induction effect. Here we see that the *Opponent Processing of Neural Receptive Fields* correctly predicts the right rectangles' shift toward yellow (Figure 16g), but incorrectly also predicts those rectangles to be perceived as more green (Figure 16e). The *Discrete Wavelet Transform in Opponent Colorspace* descriptor, the opposite; it correctly predicts the left rectangles' shift toward green (Figure 17e), but incorrectly also predicts the other rectangles to be more blue (Figure 17g).

We propose three possible causes for these inconclusive results: 1) the color descriptors are inaccurate, 2) the neurodynamical model is insufficient, 3) our analysis of the model is incomplete. At this level of experimentation, all are equally possible. We feel certain that more work needs to be done to properly parameterize the *Opponent Processing of Neural Receptive Fields* method, and have already acknowledged that the *Discrete Wavelet Transform in Opponent Colorspace* method has its shortcomings. Similarly, we have touched on the lack of neurobiological support for meaningful models of interaction between chromatically tuned neurons. Finally, it need be recognized that all of our experimental results involve the summarization of the activity a multidimensional dynamic network into 3 static dimensions of information. More meaningful methods of interpreting the activity of this network can likely be devised, and may well elucidate more optimistic results, or at the very least, avenues of improvement.

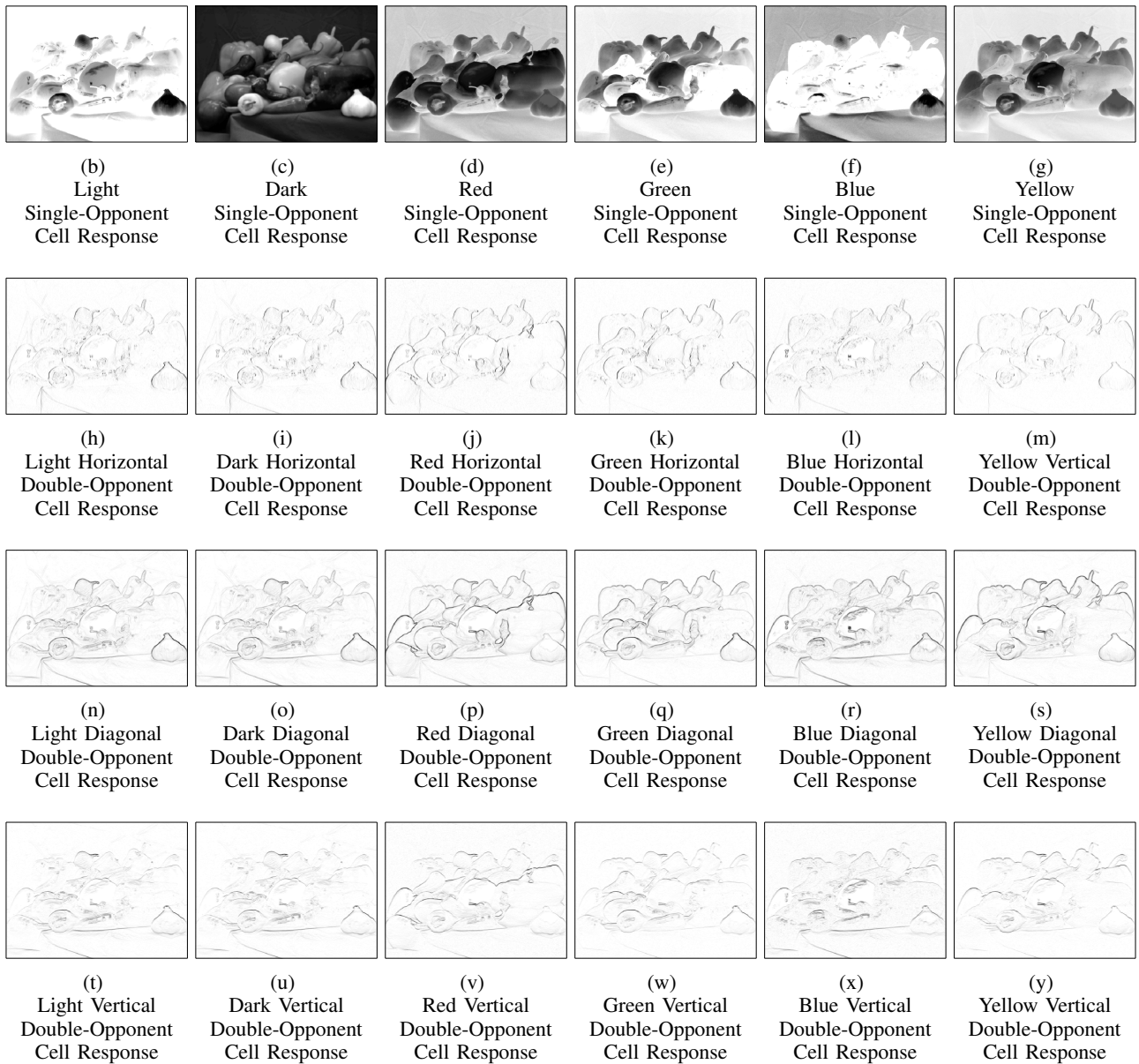
REFERENCES

- [1] Cavanaugh, J., Bair, W., and Movshon, A. *Nature and Interaction of Signals From the Receptive Field Center and Surround in Macaque V1 Neurons*. Journal of Neurophysiology 88 (2002): 2530-2546.
- [2] Conway, B., Hubel, D., and Livingstone, M. *Color Contrast in Macaque V1*. Cerebral Cortex (2002): 915-925.
- [3] Conway, B. R., S. Chatterjee, G. D. Field, G. D. Horwitz, E. N. Johnson, K. Koida, and K. Mancuso. *Advances in Color Science: From Retina to Behavior*. Journal of Neuroscience 30.45 (2010): 14955-4963.
- [4] Heeger, D. *Modeling simple-cell direction selectivity with normalized, half-squared, linear operators* Neurophysiology 70.5 (1993): 1885-1898.
- [5] Itti L., Koch C., and Niebur E. *A Model of Saliency-Based Visual Attention for Rapid Scene Analysis*. IEEE Transactions on Pattern Analysis and Machine Intelligence, 20.11 (1999). 1254-1259.
- [6] Johnson, E., Hawken, M., and Shapley, R. *The Orientation Selectivity of Color-Responsive Neurons in Macaque V1*. Journal of Neuroscience 28.32 (2008): 8096-106
- [7] Lennie, P., Haake, W., and Williams, D. *Color in the Primary Visual Cortex*. Computational Models of Visual Processing. Cambridge, Mass.: MIT, (1991): 71-82.
- [8] Li, Z. *A Neural Model of Contour Integration in the Primary Visual Cortex*. Neural Computation 10.4 (1998): 903-40.
- [9] Li, Z. *Visual Segmentation by Contextual Influences via Intra-cortical Interactions in the Primary Visual Cortex*. Network: Computation in Neural Systems 10.2 (1999): 187-212.
- [10] Li, Z. *A saliency map in primary visual cortex*. TRENDS in Cognitive Sciences 6.1 (2002): 9-16
- [11] Otazu, X., Parraga, C., and Vanrell, M. *Toward a Unified Chromatic Induction Model*. Journal of Vision 10.12 (2010): 5.
- [12] Penacchio O., Otazu, X., and Dempere-Marco, L. *A Neurodynamical Model of Brightness Induction in V1*. PLoS ONE 8.5 (2013): E64086.
- [13] Mallat, S. *A Theory for Multiresolution Signal Decomposition: The Wavelet Representation*. IEEE Transactions on Pattern Analysis and Machine Intelligence 11.7 (1989): 674-93.
- [14] Ramirez-Villegas, J., and Ramirez-Moreno, D. *Color Coding in the Cortex: A Modified Approach to Bottom-up Visual Attention*. Biological Cybernetics 107.1 (2013): 39-47.
- [15] Shapley, R., Hawken, M., and Johnson, E. *Color in the Primary Visual Cortex*. The Visual Neurosciences. Vol. 2. Cambridge, Mass.: MIT, (2004): 568-86.
- [16] Schluppeck, D., and S. A. Engel. *Color Opponent Neurons in V1: A Review and Model Reconciling Results from Imaging and Single-Unit Recording*. Journal of Vision 2.6 (2002): 480-492.
- [17] Shapley, R. and Hawken M. *Neural mechanisms for color perception in the primary visual cortex*. Current Opinion in Neurobiology 12 (2002): 426-432.
- [18] Shapley, R. and Hawken M. *Color in the Cortex: Single- and Double-opponent Cells*. Vision Research 51.7 (2011): 701-17.
- [19] Sincich, Lawrence C., and Jonathan C. Horton. *THE CIRCUITRY OF V1 AND V2: Integration of Color, Form, and Motion*. Annual Review of Neuroscience 28.1 (2005): 303-26.
- [20] Solomon, J., Sperling, G., and Chubb, C. *The Lateral Inhibition of Perceived Contrast is Indifferent to On-Center/Off-Center Segregation, but Specific to Orientation*. Vision Research 33.18 (1993): 2671-2683.
- [21] Solomon, Samuel, G., and Lennie, P. *The Machinery of Colour Vision*. Nature Reviews Neuroscience 8.4 (2007): 276-86.
- [22] Spitzer, H., Barkan, Y. *Computational adaptation model and its predictions for color induction of first and second orders*. Vision Research 45.27 (2005). 33233342.
- [23] Yang K., Gao S., Li C, and Li Y. *Efficient Color Boundary Detection with Color-opponent Mechanisms*. Computer Vision and Pattern Recognition (CVPR), (2013), pp 2810-2817.
- [24] Zhang, J., Barhomi, Y., and Serre, T. *A new biologically inspired color image descriptor*. Computer Vision ECCV 2012 Lecture Notes in Computer Science Volume 7576, (2012): 312-324.

APPENDIX



(a) Original

Figure 22: Example of single-opponent and double-opponent response (scale=1) to a test image following the *Opponent Processing of Neural Receptive Fields* workflow. Strong activity is indicated by black and weak activity by white.

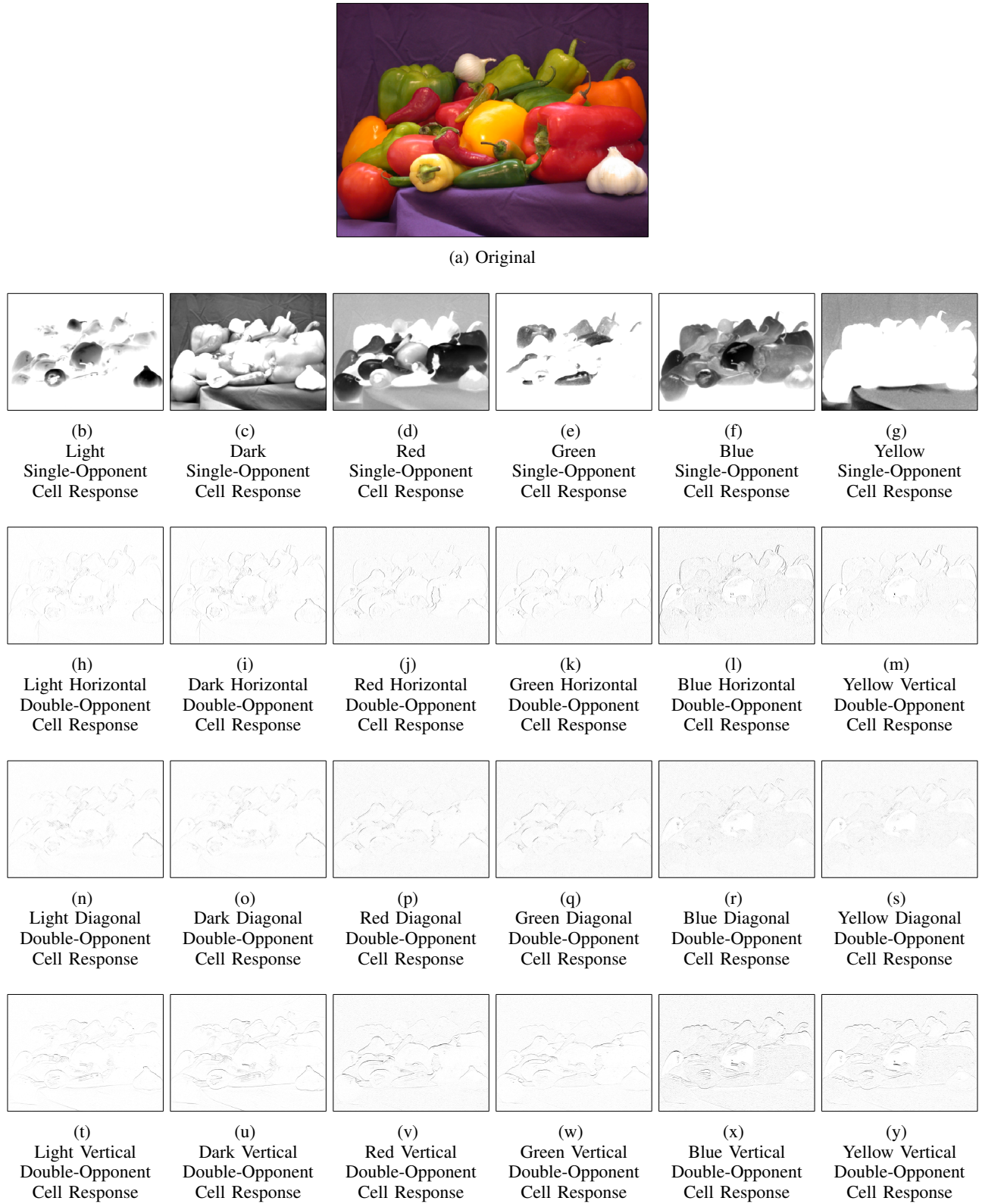


Figure 23: Example of single-opponent and double-opponent response (scale=1) to a test image following the *Discrete Wavelet Transform in Opponent Colorspace* workflow. Strong activity is indicated by black and weak activity by white.

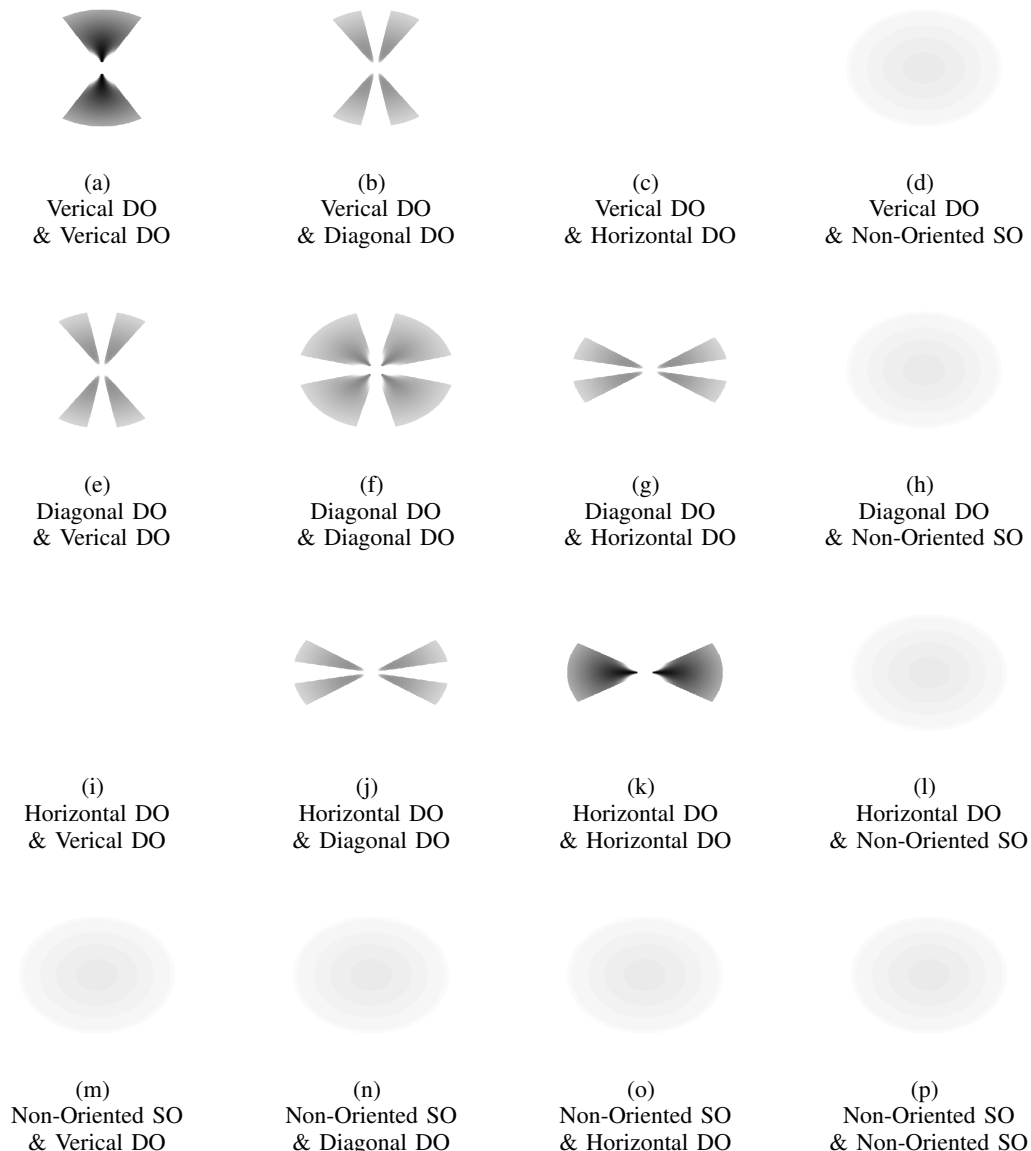


Figure 24: Graphical representation of *excitatory* interaction weights (J) between vertical, diagonal, and horizontal double-opponent cells and single-opponent cells.

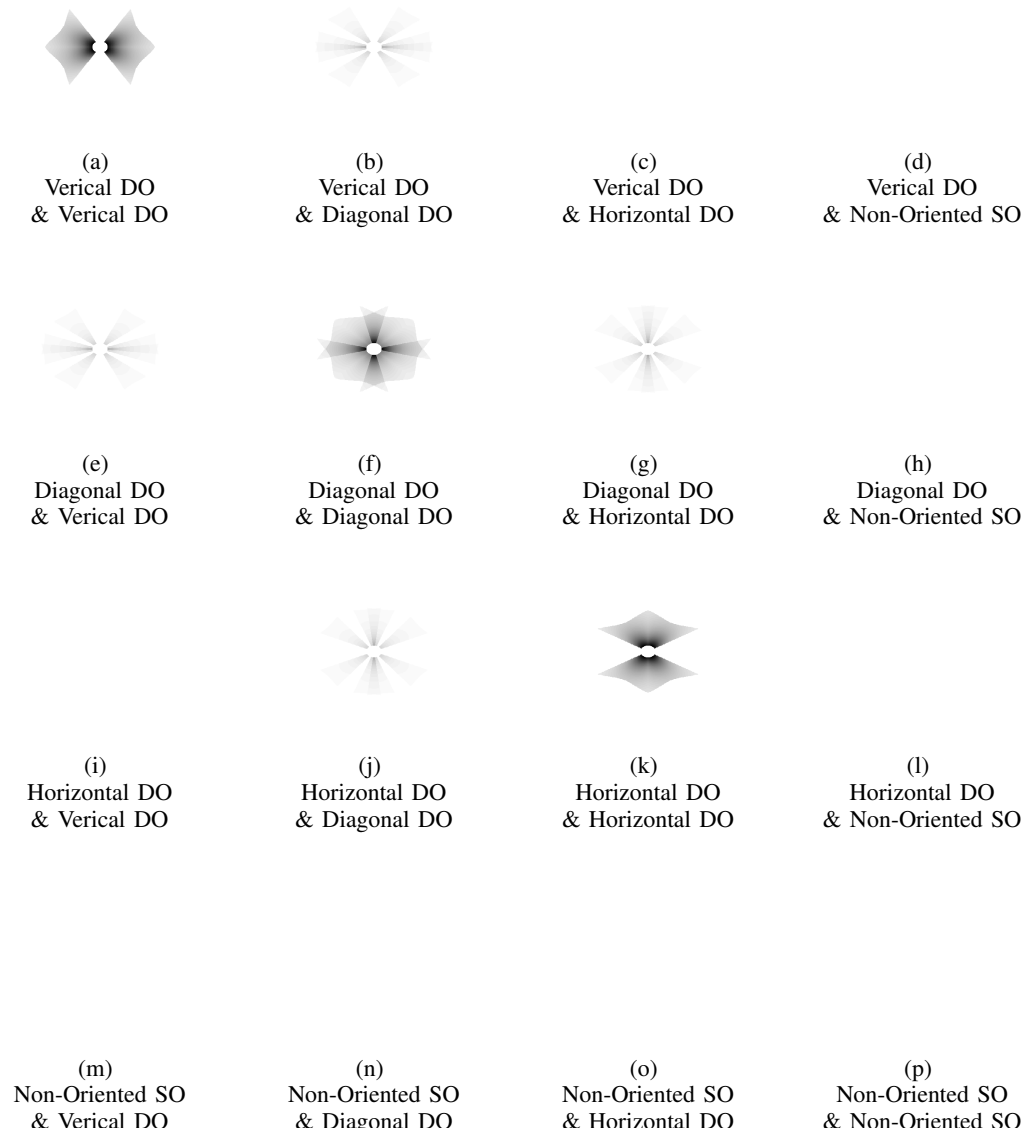


Figure 25: Graphical representation of *inhibitory* interaction weights (W) between vertical, diagonal, and horizontal double-opponent cells and single-opponent cells.